Dunlap, W.J. 2003. Crystallization Versus Cooling Ages of White Micas: Dramatic Effect of K-poor Inclusions on 40Ar/39Ar Age Spectra.
Journal of the Virtual Explorer, **13**, 54-79.

Crystallization Versus Cooling Ages of White Micas: Dramatic Effect of K-poor Inclusions on $^{40}Ar/^{39}Ar$ Age Spectra.

W. J. DUNLAP[1]

1. Research School of Earth Sciences
The Australian National University Canberra, ACT 0200
Jim.dunlap@anu.edu.au

Abstract: A strong correlation between inclusion frequency and pronounced age gradients in the $^{40}Ar/^{39}Ar$ age spectra of fine-grained mica aggregates has been discovered. Staircase age spectra generated by step heating of aggregates of micas are generally interpreted in terms of either 1) multiple populations of grains that crystallized at different times, or 2) a single population of grains that have experienced slow cooling and contain pronounced intragrain age gradients. In fine grained materials it is generally not possible to use laser ablation to explore the intragrain argon distribution, to help interpret staircase age spectra of micas. Results and observations presented here demonstrate that inclusions break up the domain structure of micas, leaving them susceptible to argon loss at temperatures lower than that of whole-crystal closure, resulting in an extremely wide range of argon retentivity. In special cases, however, age spectra with large age gradients in early gas release may still contain crystallization age information.

INTRODUCTION

Considerable progress has been made in the last twenty years towards understanding and interpreting age spectra results for step heating of bulk aggregates of micas. With the advent of laser profiling of individual mica grains (e.g., Phillips and Onstott, 1988) we were able to see for the first time the theoretically predicted intragrain age gradients of slowly cooled micas (e.g., Hodges *et al.*, 1993). Such results showed that micas tend to approximate single domains for argon diffusion and that argon transport and loss is likely to be fastest parallel to cleavage (Hames and Bowring, 1994), with strong and narrow age gradients forming at grain margins, as theoretically predicted. In addition, it has been speculated that argon diffusion and loss might also, or even preferentially, take place parallel to the c-axis micas (e.g., Lister and Baldwin, 1996), yet no conclusive evidence for this has been shown. Moreover, it became clear that natural mica grains do not generally act as theoretically perfect infinite cylinders for diffusion (e.g., Phillips and Onstott, 1988), due to the likely presence of intragrain structures that act as fast pathways for diffusion, or even open channels for argon loss (Lee, 1995; Dunlap, 1997; Kramar *et al.*, 2001; Mulch *et al.*, 2002). This characteristic of micas has consequences for thermochronology, mainly that a range of diffusion length scales and diffusivities are likely to be present in grains, and that a single closure temperature is not likely to apply, which is consistent with the "closure window" concept proposed by Dunlap (1997).

With the development of laser profiling, the method of step heating of bulk aggregates of micas was declared dead by a subsection of the community (e.g., Hodges *et al.*, 1993) for the reason that furnace heating tended to homogenise the argon release from micas, due to breakdown via dehydroxylation, yielding false plateaus. Today, there is broad agreement that step heating yields false plateaus in cases where mica populations contain significant age gradients, and that it may obscure isotopic inhomogeneity. However, the furnace step heating process does not homgenise gas release in all mica concentrates (cf. Wijbrans and McDougall, 1988), particularly in the early release before dehydroxylation is extensive. In addition, it is impossible, given the current technology, to laser profile the minute grains that characterise fine grained schists. This has made it more difficult to interpret the structural and tectonic significance of greenschist facies rocks (e.g., Lister and Raouzaios, A., 1996; Dunlap, 1998). In this regard, any new insight into the interpretation of age spectra for fine grained micas is welcome, and in this paper new findings related to the staircase-like spectra of fine grained mica aggregates are presented.

CRYSTALLIZATION VERSUS COOLING

The arguments presented in this paper revolve around two fundamentally different interpretations of the $^{40}Ar/^{39}Ar$ ages of white micas. Through dozens of studies it became clear that white micas could preserve information about either cooling or crystallization (see early work e.g., Chopin and Maluski, 1980; Kligfield *et al.*, 1986; Zingg and Hunziker, 1990; Dunlap *et al.*, 1991; see also review by Dunlap, 1997), depending both on the ambient conditions during crystallization, and the subsequent thermal history (Figure 1).

A popular interpretation by early workers, one that is still used with novel success today (e.g., Dunlap, 2000) is that micas are likely to retain information about cooling and closure of the isotopic system to significant argon loss (Dodson, 1973). There is indeed much sound evidence that supports this interpretation of "cooling ages" (cf., McDougall and Harrison, 1999). This eventually led to the general application of closure temperatures of about 300°C for biotite (Harrison *et al.*, 1985) and ~350-400 °C

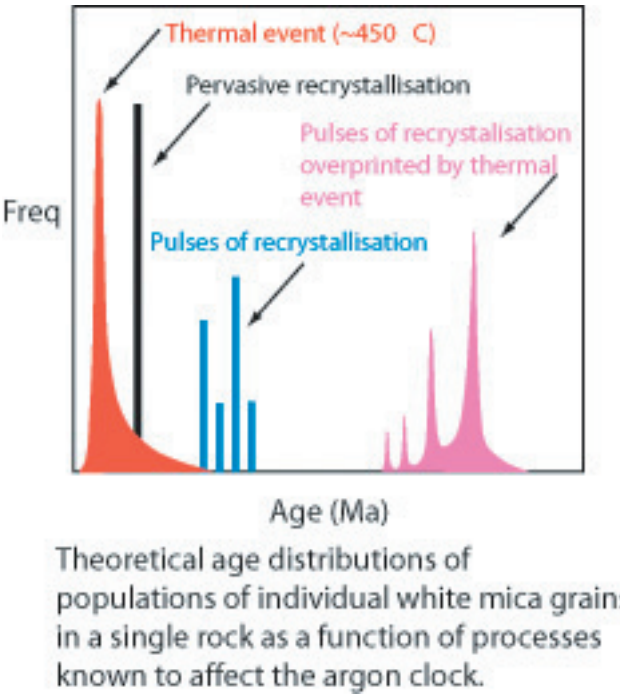

Figure 1: Synthetic histogram indicating distributions of single grain bulk ages within a hand sample, for samples that record either cooling ages, crystallization ages, or combinations of both.

for white micas (Hames and Bowring, 1994), for moderate cooling rates of a few tens of degrees Celsius per million years.

Early indications that white micas might retain their ages of crystallization, rather than cooling, were viewed with great scepticism (Chopin and Maluski, 1980), and the ensuing discussion was bitter (Desmons *et al.*, 1982). Nevertheless, as predicted by Cliff (1985), subsequent studies of white micas from deformed rocks started to yield clues that crystallization age information might be preserved in some special cases where grains formed at temperatures below their commonly accepted closure temperature (e.g., Zingg and Hunziker, 1990; Dunlap *et al.*, 1991). More recent studies of this type have shown that white micas do yield valuable structural and tectonic, crystallization age information (e.g., Dunlap *et al.*, 1995, Dunlap, 1997, Dunlap *et al.*, 1997), and that intragrain deformation alone is unlikely to enhance argon loss from micas (Dunlap and Kronenburg, 2001) unless the domain structure is segmented, yielding shorter effective diffusion dimensions (e.g., Goodwin and Renne 1991).

A set of tests to determine whether white micas from greenschist facies rocks are yielding crystallization age or cooling information have now been realised. If laser profiling cannot be utilised, one must resort to geological constraints, and comparisons with an array of independent thermal information, to make the judgement. For example, by their very nature cooling ages of mica aggregates will be much more smoothly distributed in time than crystallization ages, due to the smearing effect of diffusion (Figure 1). This is due to the fundamental physics and timescales of orogenesis, which predict that a schist can be generated in a timeframe that is much shorter than it would take to cool midcrustal rocks by conduction of heat through the Earth's surface. Thus, cooling ages will tend to vary smoothly over the regional scale of an orogen, and characterise the exhumed core (Dunlap, 2000), whereas crystallization ages will tend to correlate with and characterise particular structures (e.g., Dunlap *et al.*, 1997), particularly those on the margins of an orogen where they are unlikely to experience high temperatures during and after their development.

Thermal tests for cooling or crystallization age information come from other thermochronometers, complementary geothermometers, and mineral microstructure. For example, the Rb-Sr system of white micas is thought to have a closure temperature of around 500°C (Cliff, 1985), whereas that of the K-Ar system is around 350-400°C (Hames and Bowring, 1994). If a mica aggregate yields identical Rb-Sr and $^{40}Ar/^{39}Ar$ ages then a strong case is made that crystallization age has been recorded rather than cooling age. Obviously in the case of slow cooling the two isotopic systems would yield different ages, with the K-Ar age being younger, provided that the timescale of cooling is long enough to resolve the age difference. The K-feldspar thermochronometer has also been used successfully to differentiate between cooling and crystallization ages. Dunlap (1997) was able to identify crystallization ages in a nappe complex in part due to the presence of much older K-feldspars. This argument relied on the fact that the closure temperature of K-feldspar is lower than that of white micas. The helium thermochronometer, in zircons or titanites, for example, could be used in a similar way. An alternative indicator of cool temperatures is the preservation of certain deformation microstructures in quartz (Hirth and Tullis, 1992; Dunlap *et al.*, 1997). This approach relies on the fact that Regime 1 and Regime 2 microstructures in quartz are destroyed at high temperatures (Hirth *et al.*, 2001). The mere presence of such microstructures is a strong indication that crystallization ages in micas have been preserved. In principle this approach can be applied to other mineral systems, such as calcite and feldspars, although it has only presently been developed for quartz. New methods using Raman spectroscopy are also being developed to measure temperatures using carbonaceous matter derived from organic matter. This approach relies on the extent of development of carbon-carbon bonds, which changes strongly as a function of temperature (Beyssac *et al.*, 2002). Methods such as fission track analysis, illite crystallinity, conodont maturation, and vitrinite reflectance, offer little hope because the temperature range they access is mostly too low, or they are not optimal indicators of temperature in the greenschist facies.

Inclusions, a Potential Bane

In an ideal world we could differentiate between crystallization ages and cooling ages in fine grained mica aggregates provided that one, or preferably several, of the thermal tests could be applied with success. In practice, however, there are additional complications with fine grained aggregates that might cloud interpretations if one is not careful.

Fine grained white micas from deformed rocks, particularly those from greenschists, are difficult to concentrate by conventional mineral separation procedures (heavy liquid, magnetic, paper shaking, hand picking, etc.), for a variety of mainly physical reasons. An associated complication is that if grains cannot be sized into monomineralic grains then the combined physical properties of the composite hampers purification. Also, at very fine grain sizes the identification of contaminants requires investigation by x-ray techniques, and even pure aggregates might suffer from complications from $^{40}Ar/^{39}Ar$ analysis, such a recoil loss of ^{39}Ar. In general, however, these complications can be avoided with careful attention to detail.

One complication associated with fine grained deformed rocks that is difficult to avoid, however, is the presence of low-K inclusions in micas. Generally the presence of a volumetrically minor amount of inclusions is not a problem for $^{40}Ar/^{39}Ar$ dating, provided that little in the way of K or Ar is present in the inclusions or along their grain boundaries or in "traps". Yet the nature of the deformation process in such rocks requires that grain boundary migration and new mica growth is extensive, so some level of inclusions is unavoidable. The questions addressed in this contribution are can and will inclusions influence the shape of $^{40}Ar/^{39}Ar$ age spectra, and can they complicate the interpretation of cooling versus crystallization ages? The short answer is yes they can, as shown by data presented below.

^{40}AR/^{39}AR CASE STUDIES

$^{40}Ar/^{39}Ar$ studies of fine-grained white micas derived from greenschist facies schists have been conducted in the course of developing structural and tectonic models for both the Zhangbaling area adjacent the Tan-Lu fault in China, and the Forlandsundet Basin area of Spitzbergen, Norway. In both of these studies the grade of the deformation was low enough to consider that crystallization ages, or deformation ages, might be preserved rather than cooling ages. Significant challenges were presented in the testing of this hypothesis. In the case of the Spitzbergen micas no conclusion at all could be reached and the data was never published.

The most striking manifestation of non-standard behaviour in the Zhangbaling and Forlandsundet micas is the presence of dramatic age gradients in the $^{40}Ar/^{39}Ar$ age spectra, as shown in Figures 2 and 3. These staircase spectra are unusual for two reasons, 1) the homogenising effect of step-heating is to yield false plateaus (Hodges *et al.*, 1993), which these samples appear to have resisted, and 2) the age gradients are so large that one would expect the grain population to be markedly inhomogeneous in age, either grain to grain, or intragrain. The other common link between the micas is that they all possess some level of contamination by low-K inclusions, a not uncommon situation for metamorphic micas. The Forlandsundet samples are particularly effected by a high density of inclusions. Despite the complexity of the data, however, in both cases the range of ages correlates well with the geological history of the region, thus excess argon and alteration were ruled out as causes of the age gradients.

The driving force for this study is determining the cause of the age gradients. Age gradients in the age spectra of micas have classically been interpreted in terms of reheating events (cf., McDougall and Harrison, 1999). In such cases, the plateau-like portion of the age spectrum is considered a minimum for the original cooling age, whereas the youngest age intercept in the early gas release is considered a maximum for the age of the reheating event. In these case studies it was acknowledged that reheating could be the cause of the age gradients, yet the field evidence strongly suggested that deformation ages might be recorded. Thus, a dilemma was presented.

Zhangbaling Schist

The Zhangbaling schist forms part of the Zhangbaling metamorphic belt, situated adjacent to and southeast of the Tan-Lu strike slip fault in China (e.g., Xu, 1987). It is not useful here to give an expansive explanation of the geology except for a few salient points. The rocks selected for this study all had volcanogenic protoliths that were metamorphosed into greenschist facies mylonites and schists during transpression along the Tan-Lu fault in the Triassic. The rocks are quartz, albite, white mica schists, of greenschist grade, which contain a single well developed foliation, and a strong mineral stretching lineation. Structural synthesis of the area (Zhang *et al.*, submitted) indicates that the schists are fully recrystallised and that they formed during a single deformation.

We have applied the $^{40}Ar/^{39}Ar$ method of isotopic dating to five Zhangbaling schists with the goal of obtaining either crystallization age or cooling age information. In total, eighteen mineral separates from the five rocks were prepared and subsequently step-heated for $^{40}Ar/^{39}Ar$ analysis. In addition, K-Ar (Table 1) and Rb-Sr (Table 2) analysis were carried out on several of the mineral separates to test for complicating factors such as sample homogeneity, recoil loss of ^{39}Ar, and loss of ^{40}Ar. X- ray diffraction study of the separates was undertaken to characterize the structure of the micas and identify the composition of contaminating phases.

Five rock samples (9901, 9904, 9905A, 9905D, 9905H, 9909), composed mostly of quartz, albite and white mica, were crushed by conventional means. Sieved fractions were treated ultrasonically, briefly, and then washed in water and deslimed. This process generally removes micas below about 10 microns in cleavage-parallel diameter. Some concentration of the micas was achieved by stirring the samples in a large (5-10 liter) beaker and settling; micas tend to concentrate in the top of the sedimented column. Fractions were then subjected to centrifugation in heavy liquids of densities 2.75, 2.85 and 2.96 (± 0.01 g/cc) to remove quartz, feldspars and heavy minerals. Despite repeated centrifugation it was found that purity of the white mica concentrates ranged from ~90% to ~99%, with remaining contaminants being mostly iron oxides, quartz and albite as either inclusions or as fine-grained clusters intergrown with the white micas. The contaminants could not be removed by conventional means, but since we did not consider that these minerals would contain significant potassium or argon we pursued $^{40}Ar/^{39}Ar$ analysis.

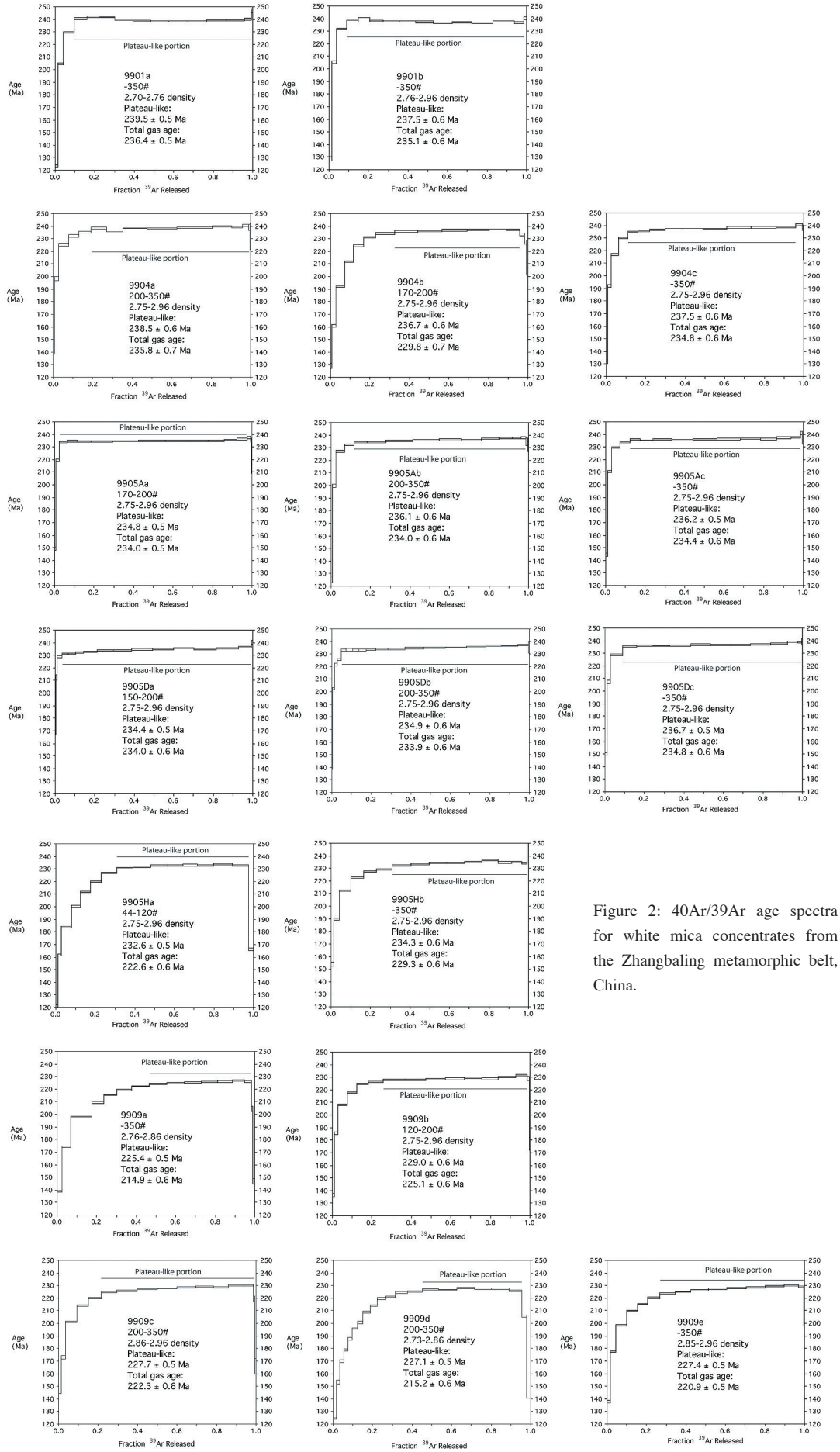

Figure 2: 40Ar/39Ar age spectra for white mica concentrates from the Zhangbaling metamorphic belt, China.

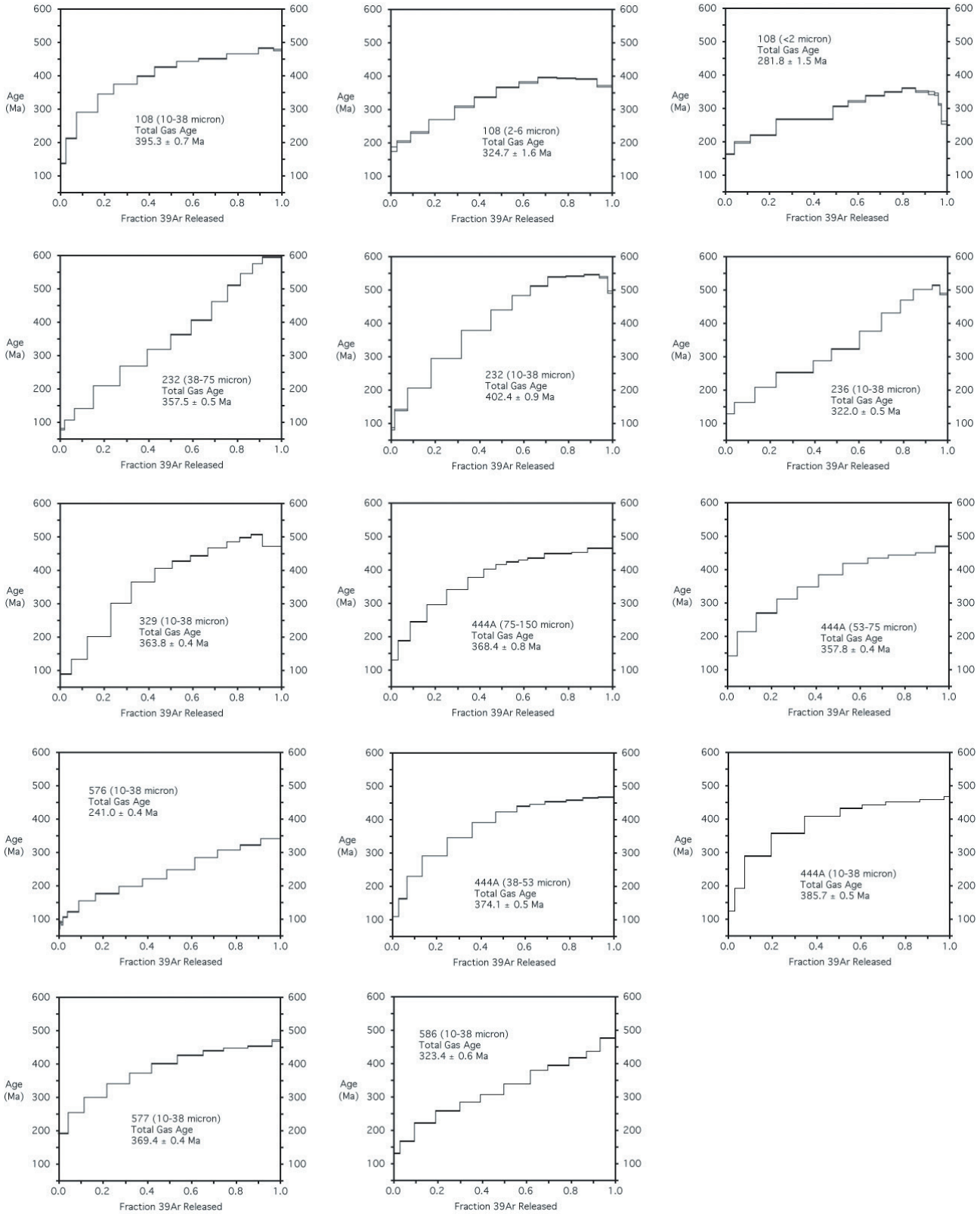

Figure 3: 40Ar/39Ar age spectra for white mica concentrates from the Forlandsundet Basin sedimentary rocks, Svalbard.

Table1. K-Ar Data for White Mica Concentrates

Sample #	Mineral	Size microns and Density fraction	K wt%	*Ar	% *Ar	Age (Ma)
9901a	musc	<45; 2.70-2.76	7.22	3.045	98.0	228 ± 3
9904a	musc	45-75; 2.75-2.96	9.27	3.908	95.8	228 ± 2
9904c	musc	<45; 2.75-2.96	8.53	3.686	94.2	234 ± 2
9905Ab	musc	45-75; 2.75-2.96	8.88	3.835	96.9	233 ± 2
9905Ac	musc	<45; 2.75-2.96	8.96	3.798	93.8	229 ± 2
9905Da	musc	75-104; 2.75-2.96	9.29	3.980	99.2	232 ± 2
9905Dc	musc	<45; 2.75-2.96	8.14	3.479	96.2	231 ± 2
9905Hb	musc	<45; 2.75-2.96	8.42	3.452	91.2	222 ± 2
9909a	musc	<45; 2.76-2.86	7.08	2.729	81.4	210 ± 2
9909b	musc	75-124; 2.75-2.96	9.06	3.645	97.7	218 ± 2
9909c	musc	45-75; 2.86-2.96	8.70	3.434	95.9	214 ± 2

*Ar is radiogenic argon of isotopic mass 40 in units of 1×10^{-9} mol/g. K = potassium; values are means of two dissolutions of each concentrate. $\%^{40}Ar^*$ is percent radiogenic argon of isotopic mass 40. Decay constants are $\lambda_e = 0.581 \times 10^{-10} y^{-1}$ and $\lambda_\beta = 4.962\ 10^{-10} y^{-1}$.

Table 2 Rb/Sr Data for White Mica Concentrates

Sample #	Mineral	Rb (ppm)	Sr (ppm)	$^{87}Rb/^{86}Sr$	$^{87}Sr/^{86}Sr$	Age (Ma)
9904a	musc	343	9.89	103.8	1.0501	230 ± 5
9905Ab	musc	436	7.26	184.0	1.3076	228 ± 5
9905Dc	musc	326	8.36	116.9	1.0954	232 ± 5

See Appendix for analytical details

The results of $^{40}Ar/^{39}Ar$ step-heating are shown in Figure 2 for mica concentrates from five Zhangbaling schists, samples 9901, 9904, 9905A, 9905D, 9905H, and 9909. In this figure each of the eighteen concentrates are identified by the last lower-case letter in the sample name (e.g., 9901a and 9901b). Note that from 2-5 mica concentrates, including either two or three grain size fractions, and in some cases different density fractions (e.g., 2.76-2.85 g/cc or 2.86-2.96 g/cc), have been analysed for each sample. The broad characteristics of the age spectra are immediately obvious in Figure 2, with some samples typified by rising, staircase spectra, and others by plateau-like spectra. Moreover, no correlation between grain size and age is indicated, suggesting that the results are more consistent with crystallization ages rather than cooling ages.

The details of each analysis are presented in Table 3. In general the calculated K/Ca for all the concentrates is in the thousands, indicating essentially no contamination by feldspars. Thus, the age gradients are clearly not a result of argon derived from feldspar within the mica concentrates. The calculated Cl/K of the concentrates is generally around 0.003 and uniform across gas release, suggesting that fluid inclusions rich in chlorine are insignificant. Isochron analysis did not yield useful information, as the samples are too radiogenic.

White mica concentrates from samples 9901, 9904, 9905A and 9905D exhibit age spectra with plateau-like sections for ~80-95% of gas release, with the exception of concentrate 9904b. In these cases the age of the evolved gas rises quickly with increasing temperature, from late Mesozoic ages, to ages that are Triassic. For these eleven mica concentrates the plateau-like sections form a remarkably narrow range in age from 234.4 Ma to 239.5 Ma, spanning just over 2%. Total gas ages are generally only 1% less than the plateau-like ages. Concentrates from a given sample yield plateau-like sections that span an even narrower range in age. The mean of plateau-like ages are 9901 = 238.5 ± 1.4 Ma, 9904 = 237.6 ± 0.9 Ma, 9905A = 235.7 ± 0.8 Ma, and 9905D = 235.3 ± 1.2 Ma, indicating remarkable intrasample homogeneity (error expressed at one Std Dev on the mean). It is interesting to note that although the age gradient in concentrate 9904b is more pronounced than any other sample in this group, and that its total gas age is much lower, the age exhibited by the plateau-like section is still within error of the mean of the three subfractions of 9904. This suggests that an age gradient of the order exhibited by sample 9904b, if it is related to argon loss, has had little affect on the plateau-like age.

White mica concentrates from samples 9909 and 9905H exhibit pronounced age gradients at the beginning of

Table 3. 40Ar/39Ar Step Heating Data for Zhangbaling White Micas.

Temp (˚C)	Ar^{36} (mol)	Ar^{37} (mol)	Ar^{38} (mol)	Ar^{39} (mol)	Ar^{40} (mol)	% Radiogenic ^{40}Ar	$^{40}Ar^*/^{39}Ar$	Cum ^{39}Ar	Age (Ma)	± 1s.d. (Ma)	Ca/K	Cl/K
9901a												
600	400.17E-	285.17E-	217.16E-	206.15E-	432.14E-	72.5	15.22	1.5	123.5	0.8	26.32E-	42.84E-
700	399.17E-	804.17E-	393.16E-	372.15E-	108.13E-	89	25.79	4.1	204.6	0.8	41.12E-	91.64E-
780	420.17E-	102.16E-	842.16E-	762.15E-	235.13E-	94.6	29.14	9.6	229.6	0.6	25.32E-	22.93E-
830	273.17E-	160.16E-	105.15E-	907.15E-	286.13E-	97.1	30.65	16	240.7	0.7	33.52E-	36.33E-
860	186.17E-	163.16E-	105.15E-	924.15E-	291.13E-	98	30.83	22.6	242	0.6	33.62E-	31.63E-
890	158.17E-	772.17E-	121.15E-	107.14E-	334.13E-	98.5	30.78	30.3	241.6	0.5	13.72E-	30.73E-
920	166.17E-	121.16E-	144.15E-	128.14E-	397.13E-	98.7	30.51	39.4	239.7	0.5	18.02E-	28.73E-
940	166.17E-	120.16E-	138.15E-	124.14E-	383.13E-	98.6	30.38	48.3	238.7	0.6	18.32E-	26.03E-
960	189.17E-	296.16E-	142.15E-	130.14E-	398.13E-	98.5	30.29	57.5	238	0.5	43.42E-	23.33E-
980	168.17E-	528.16E-	148.15E-	134.14E-	412.13E-	98.7	30.29	67.1	238	0.6	74.72E-	24.33E-
1000	187.17E-	447.16E-	150.15E-	136.14E-	419.13E-	98.6	30.32	76.8	238.3	0.4	62.22E-	23.33E-
1020	194.17E-	276.16E-	153.15E-	138.14E-	425.13E-	98.6	30.43	86.6	239.1	0.4	38.22E-	26.43E-
1050	209.17E-	383.16E-	145.15E-	132.14E-	409.13E-	98.4	30.43	96.1	239.1	0.5	55.02E-	23.33E-
1080	182.17E-	656.16E-	514.16E-	465.15E-	147.13E-	96.3	30.57	99.4	240.1	0.7	26.81E-	24.33E-
1140	188.17E-	101.15E-	883.17E-	755.16E-	292.14E-	81.3	31.46	99.9	246.7	1.8	25.50E+	30.33E-
1350	350.17E-	101.15E-	224.17E-	124.16E-	157.14E-	34.6	44.04	100	336.6	22.1	15.51E+	68.43E-
								Total	236.4	0.5		
9901b												
600	289.17E-	278.19E-	146.16E-	135.15E-	300.14E-	71.4	15.88	1.3	128.7	1.5	39.24E-	10.13E-
700	346.17E-	129.16E-	259.16E-	240.15E-	726.14E-	85.8	25.93	3.7	205.6	1.1	10.21E-	12.53E-
780	279.17E-	415.17E-	582.16E-	511.15E-	159.13E-	94.7	29.44	8.8	231.7	0.7	15.42E-	31.73E-
830	224.17E-	142.17E-	693.16E-	609.15E-	191.13E-	96.4	30.27	14.9	237.8	0.8	44.33E-	32.33E-
860	154.17E-	472.17E-	680.16E-	587.15E-	184.13E-	97.4	30.6	20.7	240.3	0.6	15.32E-	37.43E-
890	141.17E-	260.17E-	779.16E-	684.15E-	212.13E-	97.9	30.31	27.5	238.1	0.6	72.23E-	32.83E-
920	140.17E-	326.17E-	929.16E-	824.15E-	254.13E-	98.3	30.27	35.7	237.8	0.6	75.23E-	30.23E-
940	125.17E-	832.17E-	929.16E-	827.15E-	254.13E-	98.5	30.24	43.9	237.6	0.6	19.12E-	29.63E-
960	146.17E-	278.19E-	100.15E-	885.15E-	272.13E-	98.3	30.18	52.7	237.2	0.8	59.85E-	30.93E-
980	167.17E-	205.16E-	106.15E-	950.15E-	291.13E-	98.2	30.1	62.2	236.6	0.7	41.02E-	27.03E-
1000	149.17E-	121.16E-	114.15E-	102.14E-	311.13E-	98.5	30.19	72.3	237.3	0.5	22.72E-	28.23E-
1020	168.17E-	705.17E-	122.15E-	108.14E-	331.13E-	98.4	30.11	83	236.7	0.6	12.42E-	29.93E-
1050	169.17E-	175.16E-	123.15E-	110.14E-	338.13E-	98.4	30.27	94	237.9	0.5	30.32E-	29.23E-
1080	157.17E-	239.16E-	540.16E-	484.15E-	151.13E-	96.8	30.12	98.8	236.8	0.8	93.82E-	26.93E-
1140	156.17E-	443.16E-	125.16E-	113.15E-	390.14E-	88.2	30.62	99.9	240.4	1.1	74.91E-	21.13E-
1350	312.17E-	706.16E-	292.17E-	994.17E-	133.14E-	31.1	41.84	100	321.1	27.4	13.61E+	32.92E-
								Total	235.2	0.6		
9904a												
600	396.17E-	243.19E-	743.17E-	650.16E-	231.14E-	49.3	17.52	0.8	141.1	3.1	70.94E-	69.44E-
700	401.17E-	203.17E-	158.16E-	147.15E-	488.14E-	75.6	25.07	2.6	198.6	1.7	26.22E-	56.54E-
800	405.17E-	694.18E-	487.16E-	440.15E-	138.13E-	91.3	28.68	7.9	225.5	1	29.93E-	21.83E-
850	233.17E-	477.18E-	454.16E-	407.15E-	127.13E-	94.5	29.62	12.9	232.4	1	22.33E-	25.63E-
890	215.17E-	243.19E-	573.16E-	513.15E-	160.13E-	95.9	29.99	19.1	235.2	1	90.15E-	26.83E-
920	184.17E-	243.19E-	721.16E-	650.15E-	203.13E-	97.2	30.43	27	238.3	0.7	71.15E-	25.53E-
940	207.17E-	243.19E-	753.16E-	690.15E-	214.13E-	97.1	30.16	35.3	236.4	0.8	67.05E-	20.93E-
970	186.17E-	134.17E-	109.15E-	997.15E-	309.13E-	98.1	30.45	47.4	238.5	0.5	25.53E-	21.93E-
1000	271.17E-	555.17E-	136.15E-	125.14E-	387.13E-	97.8	30.39	62.6	238.1	0.5	84.63E-	21.93E-
1030	284.17E-	102.17E-	163.15E-	148.14E-	459.13E-	98.1	30.48	80.5	238.7	0.5	13.23E-	23.83E-
1050	240.17E-	245.19E-	917.16E-	829.15E-	261.13E-	97.2	30.62	90.5	239.8	0.6	56.15E-	24.53E-
1070	215.17E-	245.19E-	484.16E-	439.15E-	141.13E-	95.4	30.55	95.9	239.3	0.7	10.64E-	22.73E-
1100	214.17E-	245.19E-	276.16E-	248.15E-	825.14E-	92.2	30.75	98.9	240.7	0.7	18.84E-	24.53E-
1160	266.17E-	136.17E-	772.17E-	643.16E-	275.14E-	71.3	30.52	99.7	239	2.4	40.12E-	29.93E-
1350	479.17E-	365.17E-	429.17E-	288.16E-	227.14E-	37.5	29.54	100	231.8	10.3	24.11E-	42.83E-
								Total	235.8	0.7		

Temp (˚C)	Ar^{36} (mol)	Ar^{37} (mol)	Ar^{38} (mol)	Ar^{39} (mol)	Ar^{40} (mol)	% Radiogenic ^{40}Ar	$^{40}Ar^*/^{39}Ar$	Cum 39Ar	Age (Ma)	± 1s.d. (Ma)	Ca/K	Cl/K
9904b												
600	382.17E-	137.17E-	912.17E-	797.16E-	240.14E-	52.8	15.92	0.8	129	2.2	32.62E-	13.33E-
700	252.17E-	192.17E-	188.16E-	164.15E-	404.14E-	81.5	20.05	2.6	160.9	1	22.22E-	29.03E-
800	314.17E-	380.17E-	479.16E-	423.15E-	111.13E-	91.6	24.1	7.1	191.9	0.6	17.12E-	29.23E-
850	185.17E-	262.19E-	474.16E-	422.15E-	119.13E-	95.3	26.8	11.5	212.1	0.5	11.84E-	27.93E-
890	162.17E-	262.19E-	544.16E-	484.15E-	143.13E-	96.5	28.45	16.6	224.4	0.8	10.34E-	29.03E-
920	159.17E-	890.17E-	653.16E-	585.15E-	177.13E-	97.3	29.37	22.8	231.2	0.7	28.92E-	26.93E-
950	187.17E-	225.16E-	102.15E-	930.15E-	283.13E-	98	29.76	32.7	234	0.7	45.92E-	23.83E-
970	190.17E-	208.16E-	120.15E-	108.14E-	329.13E-	98.2	30	44	235.8	0.6	36.72E-	26.23E-
990	194.17E-	249.16E-	131.15E-	117.14E-	359.13E-	98.3	30.05	56.4	236.2	0.6	40.32E-	27.13E-
1010	188.17E-	181.16E-	133.15E-	119.14E-	365.13E-	98.4	30.13	69.1	236.8	0.7	28.92E-	26.73E-
1030	195.17E-	240.16E-	119.15E-	107.14E-	328.13E-	98.2	30.19	80.3	237.3	0.5	42.82E-	27.53E-
1050	177.17E-	431.16E-	905.16E-	823.15E-	254.13E-	97.9	30.21	89	237.4	0.5	99.42E-	23.33E-
1080	188.17E-	623.16E-	707.16E-	642.15E-	199.13E-	97.2	30.17	95.8	237.1	0.6	18.51E-	23.33E-
1110	166.17E-	468.16E-	261.16E-	239.15E-	759.14E-	93.5	29.68	98.3	233.5	1	37.21E-	18.93E-
1160	198.17E-	676.16E-	946.17E-	842.16E-	301.14E-	80.7	28.88	99.2	227.5	1.7	15.30E+	19.53E-
1350	353.17E-	613.16E-	837.17E-	725.16E-	290.14E-	64.2	25.68	100	203.7	2.4	16.10E+	15.33E-
								Total	229.8	0.7		
9904c												
600	265.17E-	351.17E-	961.17E-	861.16E-	219.14E-	64.1	16.28	0.9	131.6	1.7	77.42E-	14.13E-
700	288.17E-	403.17E-	174.16E-	162.15E-	478.14E-	82.1	24.17	2.5	192.1	1.1	47.22E-	92.94E-
780	323.17E-	135.17E-	422.16E-	380.15E-	114.13E-	91.5	27.51	6.2	217.1	0.7	67.43E-	22.73E-
830	232.17E-	267.19E-	557.16E-	494.15E-	152.13E-	95.4	29.24	11.1	229.9	0.5	10.34E-	28.53E-
860	170.17E-	267.19E-	569.16E-	507.15E-	157.13E-	96.7	29.94	16.1	235	0.7	10.04E-	28.53E-
890	160.17E-	267.19E-	677.16E-	605.15E-	187.13E-	97.4	30.03	22.1	235.7	0.6	83.85E-	27.53E-
920	174.17E-	267.19E-	886.16E-	793.15E-	245.13E-	97.8	30.17	29.9	236.8	0.5	64.05E-	27.73E-
940	175.17E-	280.17E-	980.16E-	879.15E-	271.13E-	98	30.24	38.6	237.2	0.5	60.53E-	27.03E-
960	175.17E-	267.19E-	116.15E-	105.14E-	324.13E-	98.3	30.21	49	237.1	0.6	48.25E-	24.13E-
980	202.17E-	132.16E-	132.15E-	120.14E-	370.13E-	98.3	30.26	60.9	237.4	0.4	20.82E-	23.33E-
1000	196.17E-	268.19E-	140.15E-	128.14E-	394.13E-	98.4	30.39	73.4	238.4	0.7	39.95E-	23.53E-
1020	219.17E-	411.17E-	140.15E-	128.14E-	396.13E-	98.3	30.4	86.1	238.4	0.6	61.13E-	22.63E-
1050	217.17E-	964.17E-	110.15E-	101.14E-	313.13E-	97.9	30.42	96	238.6	0.7	18.22E-	21.03E-
1080	153.17E-	105.17E-	357.16E-	323.15E-	104.13E-	95.6	30.68	99.2	240.5	0.8	61.83E-	23.43E-
1140	173.17E-	439.17E-	705.17E-	621.16E-	240.14E-	78.6	30.37	99.8	238.2	2.4	13.41E-	20.03E-
1350	354.17E-	112.16E-	284.17E-	193.16E-	159.14E-	34.1	28.11	100	221.5	8.5	11.10E+	31.93E-
								Total	234.8	0.6		
9905Aa												
600	241.17E-	283.19E-	149.16E-	139.15E-	330.14E-	78.3	18.56	0.8	149.4	1.2	38.54E-	90.84E-
700	194.17E-	283.19E-	282.16E-	259.15E-	778.14E-	92.5	27.84	2.3	219.7	0.7	20.84E-	18.43E-
800	288.17E-	283.19E-	876.16E-	770.15E-	238.13E-	96.3	29.76	6.6	233.9	0.6	69.85E-	32.13E-
850	196.17E-	283.19E-	998.16E-	871.15E-	266.13E-	97.7	29.86	11.6	234.7	0.6	61.75E-	34.43E-
890	181.17E-	283.19E-	141.15E-	124.14E-	377.13E-	98.5	29.81	18.6	234.3	0.4	43.25E-	31.43E-
920	201.17E-	283.19E-	213.15E-	189.14E-	570.13E-	98.9	29.81	29.4	234.3	0.6	28.55E-	30.53E-
950	316.17E-	283.19E-	259.15E-	229.14E-	693.13E-	98.6	29.85	42.4	234.6	0.4	23.55E-	31.63E-
970	226.17E-	284.19E-	274.15E-	242.14E-	731.13E-	99	29.88	56.1	234.9	0.5	22.35E-	31.73E-
990	201.17E-	284.19E-	231.15E-	206.14E-	622.13E-	99	29.91	67.8	235	0.5	26.25E-	29.33E-
1010	194.17E-	284.19E-	195.15E-	174.14E-	526.13E-	98.8	29.91	77.7	235	0.5	31.05E-	28.93E-
1030	181.17E-	284.19E-	163.15E-	146.14E-	441.13E-	98.7	29.89	86	234.9	0.4	37.05E-	28.33E-
1050	163.17E-	284.19E-	131.15E-	118.14E-	358.13E-	98.6	30.01	92.6	235.8	0.5	45.85E-	26.63E-
1080	156.17E-	284.19E-	977.16E-	874.15E-	267.13E-	98.2	30.05	97.6	236.1	0.8	61.85E-	27.93E-
1110	127.17E-	284.19E-	325.16E-	288.15E-	911.14E-	95.8	30.29	99.2	237.8	1.1	18.74E-	29.13E-
1160	155.17E-	271.17E-	103.16E-	909.16E-	318.14E-	85.6	29.95	99.7	235.4	1.6	56.62E-	25.53E-
1350	289.17E-	394.17E-	540.17E-	457.16E-	208.14E-	59	26.93	100	212.9	3.6	16.41E-	15.83E-
								Total	234	0.5		

Temp	Ar^{36}	Ar^{37}	Ar^{38}	Ar^{39}	Ar^{40}	% Radiogenic	$^{40}Ar^*/^{39}Ar$	Cum	Age	± 1s.d.	Ca/K	Cl/K

(˚C)	(mol)	(mol)	(mol)	(mol)	(mol)	^{40}Ar		^{39}Ar	(Ma)	(Ma)		
9905Ab												
600	232.17E-	148.18E-	113.16E-	105.15E-	231.14E-	70.2	15.5	0.8	125.5	2.7	26.93E-	84.94E-
700	234.17E-	246.19E-	219.16E-	198.15E-	568.14E-	87.7	25.15	2.3	199.6	1.4	23.54E-	20.43E-
800	265.17E-	246.19E-	652.16E-	576.15E-	174.13E-	95.4	28.83	6.7	227	0.8	81.15E-	30.33E-
850	208.17E-	123.17E-	723.16E-	633.15E-	193.13E-	96.7	29.54	11.6	232.2	0.6	36.93E-	33.23E-
890	183.17E-	145.17E-	956.16E-	852.15E-	260.13E-	97.8	29.85	18.1	234.5	0.6	32.33E-	28.83E-
920	232.17E-	246.19E-	139.15E-	124.14E-	378.13E-	98.1	29.83	27.6	234.4	0.5	37.75E-	28.73E-
950	240.17E-	246.19E-	203.15E-	182.14E-	553.13E-	98.6	29.99	41.6	235.6	0.5	25.75E-	28.03E-
970	175.17E-	418.19E-	193.15E-	172.14E-	523.13E-	98.9	30.06	54.8	236.1	0.5	46.15E-	28.53E-
990	255.17E-	418.19E-	162.15E-	146.14E-	449.13E-	98.2	30.09	66	236.3	0.7	54.25E-	24.33E-
1010	236.17E-	418.19E-	148.15E-	132.14E-	403.13E-	98.2	30.04	76.1	235.9	0.7	60.35E-	28.43E-
1030	236.17E-	418.19E-	127.15E-	114.14E-	351.13E-	97.9	30.22	84.8	237.2	0.5	69.95E-	28.13E-
1050	130.17E-	247.19E-	991.16E-	894.15E-	275.13E-	98.5	30.28	91.7	237.7	0.5	52.65E-	25.83E-
1070	219.17E-	247.19E-	677.16E-	610.15E-	191.13E-	96.5	30.26	96.4	237.6	0.6	77.05E-	25.03E-
1100	240.17E-	247.19E-	355.16E-	315.15E-	103.13E-	93	30.34	98.8	238.1	0.8	14.94E-	27.03E-
1160	276.17E-	519.17E-	113.16E-	940.16E-	363.14E-	77.5	29.89	99.5	234.8	3	10.51E-	36.73E-
1350	469.17E-	113.16E-	818.17E-	651.16E-	330.14E-	58	29.37	100	231	4.1	32.81E-	29.63E-
							Total		234	0.6		
9905Ac												
600	224.17E-	560.17E-	113.16E-	107.15E-	258.14E-	74.2	17.92	1.1	144.4	1.5	99.82E-	43.14E-
700	215.17E-	272.19E-	221.16E-	195.15E-	584.14E-	89	26.63	3.1	210.6	0.8	26.44E-	26.43E-
780	230.17E-	272.19E-	469.16E-	409.15E-	126.13E-	94.5	29.19	7.2	229.6	0.6	12.64E-	33.33E-
830	189.17E-	364.17E-	575.16E-	497.15E-	154.13E-	96.3	29.79	12.3	234	0.6	13.92E-	36.73E-
860	155.17E-	272.19E-	583.16E-	507.15E-	157.13E-	97	30.03	17.5	235.8	0.6	10.24E-	34.73E-
890	159.17E-	102.17E-	748.16E-	653.15E-	201.13E-	97.6	29.94	24.1	235.2	0.5	29.83E-	34.23E-
920	166.17E-	272.19E-	105.15E-	936.15E-	286.13E-	98.2	30.05	33.6	236	0.6	55.35E-	28.53E-
940	164.17E-	273.19E-	117.15E-	105.14E-	320.13E-	98.4	29.99	44.3	235.6	0.6	49.45E-	27.73E-
960	188.17E-	487.18E-	135.15E-	120.14E-	365.13E-	98.4	30.04	56.4	235.9	0.4	77.44E-	30.83E-
980	192.17E-	273.19E-	131.15E-	117.14E-	358.13E-	98.3	30.09	68.3	236.3	0.6	44.35E-	27.63E-
1000	182.17E-	273.19E-	110.15E-	987.15E-	303.13E-	98.1	30.11	78.4	236.4	0.5	52.55E-	27.53E-
1020	169.17E-	273.19E-	909.16E-	809.15E-	249.13E-	97.9	30.1	86.6	236.3	0.6	64.15E-	29.23E-
1050	166.17E-	156.17E-	803.16E-	717.15E-	222.13E-	97.7	30.24	93.9	237.4	0.7	41.33E-	28.03E-
1080	162.17E-	273.19E-	514.16E-	457.15E-	143.13E-	96.6	30.26	98.5	237.5	0.5	11.44E-	28.73E-
1140	174.17E-	273.19E-	129.16E-	113.15E-	399.14E-	87	30.77	99.7	241.3	1.3	46.14E-	28.03E-
1350	356.17E-	760.17E-	432.17E-	322.16E-	202.14E-	48	30.09	100	236.2	4.2	44.81E-	32.03E-
							Total		234.4	0.6		
9905Da												
600	188.17E-	256.19E-	550.17E-	464.16E-	155.14E-	64.1	21.45	0.4	169.7	2.5	10.53E-	26.23E-
700	184.17E-	319.17E-	979.17E-	901.16E-	299.14E-	81.7	27.16	1.1	212.4	2	67.32E-	11.83E-
800	232.17E-	256.19E-	341.16E-	312.15E-	986.14E-	93	29.39	3.5	228.7	0.7	15.64E-	19.23E-
850	171.17E-	257.19E-	416.16E-	367.15E-	114.13E-	95.5	29.74	6.4	231.3	0.6	13.34E-	30.63E-
890	149.17E-	353.17E-	536.16E-	480.15E-	147.13E-	96.9	29.73	10.1	231.2	0.5	14.02E-	27.43E-
920	164.17E-	257.19E-	629.16E-	568.15E-	175.13E-	97.1	29.86	14.5	232.2	0.5	86.05E-	25.23E-
950	182.17E-	257.19E-	921.16E-	839.15E-	257.13E-	97.8	29.96	21.1	232.9	0.5	58.25E-	23.03E-
970	193.17E-	569.18E-	115.15E-	105.14E-	322.13E-	98.1	30.07	29.3	233.7	0.6	10.33E-	22.03E-
990	215.17E-	257.19E-	129.15E-	118.14E-	363.13E-	98.2	30.1	38.5	233.9	0.5	41.25E-	20.43E-
1010	216.17E-	257.19E-	150.15E-	137.14E-	421.13E-	98.4	30.21	49.2	234.7	0.7	35.75E-	21.83E-
1030	214.17E-	257.19E-	149.15E-	137.14E-	420.13E-	98.4	30.25	59.9	235	0.5	35.85E-	21.83E-
1050	202.17E-	257.19E-	143.15E-	131.14E-	405.13E-	98.4	30.36	70.1	235.8	0.5	37.35E-	20.73E-
1080	227.17E-	454.17E-	160.15E-	146.14E-	449.13E-	98.4	30.27	81.5	235.2	0.5	59.13E-	22.23E-
1110	221.17E-	258.19E-	155.15E-	143.14E-	440.13E-	98.4	30.31	92.7	235.5	0.5	34.35E-	20.63E-
1160	204.17E-	258.19E-	927.16E-	852.15E-	266.13E-	97.6	30.46	99.3	236.5	0.6	57.55E-	20.53E-
1350	342.17E-	599.17E-	104.16E-	880.16E-	374.14E-	72.9	30.97	100	240.2	1.6	12.91E-	27.13E-
							Total		234	0.6		

Temp (˚C)	Ar^{36} (mol)	Ar^{37} (mol)	Ar^{38} (mol)	Ar^{39} (mol)	Ar^{40} (mol)	% Radiogenic ^{40}Ar	$^{40}Ar^*/^{39}Ar$	Cum ^{39}Ar	Age (Ma)	± 1s.d. (Ma)	Ca/K	Cl/K
9905Db												
600	274.17E-	157.17E-	712.17E-	642.16E-	195.14E-	58.4	17.74	0.4	142.2	4	46.52E-	68.94E-
700	217.17E-	240.19E-	159.16E-	147.15E-	441.14E-	85.4	25.66	1.4	202.3	0.9	31.14E-	13.73E-
750	156.17E-	168.17E-	200.16E-	185.15E-	570.14E-	91.8	28.27	2.6	221.6	1.2	17.22E-	15.63E-
800	216.17E-	240.19E-	339.16E-	305.15E-	941.14E-	93.1	28.77	4.6	225.3	0.8	15.04E-	23.93E-
840	167.17E-	258.18E-	462.16E-	407.15E-	126.13E-	96	29.83	7.3	233.1	0.9	12.03E-	31.23E-
870	151.17E-	241.19E-	526.16E-	475.15E-	146.13E-	96.9	29.86	10.5	233.3	1	96.25E-	24.63E-
890	186.17E-	241.19E-	550.16E-	492.15E-	152.13E-	96.3	29.83	13.7	233.1	0.8	93.05E-	27.03E-
910	162.17E-	454.17E-	641.16E-	571.15E-	175.13E-	97.2	29.84	17.5	233.2	0.8	15.12E-	28.73E-
930	178.17E-	416.18E-	823.16E-	742.15E-	227.13E-	97.6	29.86	22.4	233.3	0.7	10.63E-	25.83E-
950	269.17E-	241.19E-	103.15E-	933.15E-	287.13E-	97.1	29.92	28.5	233.7	0.5	49.15E-	23.43E-
970	236.17E-	241.19E-	137.15E-	126.14E-	383.13E-	98.1	29.97	36.8	234.1	0.6	36.55E-	20.93E-
990	262.17E-	241.19E-	161.15E-	147.14E-	449.13E-	98.2	30.05	46.5	234.7	0.7	31.25E-	23.63E-
1010	347.17E-	506.17E-	181.15E-	165.14E-	508.13E-	97.9	30.09	57.5	235	0.5	58.13E-	22.63E-
1030	242.17E-	241.19E-	175.15E-	160.14E-	488.13E-	98.4	30.12	68	235.3	0.5	28.75E-	22.53E-
1050	292.17E-	241.19E-	165.15E-	150.14E-	462.13E-	98	30.14	77.9	235.4	0.5	30.55E-	23.53E-
1070	326.17E-	242.19E-	137.15E-	124.14E-	386.13E-	97.4	30.29	86.1	236.5	0.4	37.05E-	24.63E-
1100	253.17E-	242.19E-	133.15E-	121.14E-	374.13E-	97.9	30.28	94.1	236.4	0.4	38.05E-	23.13E-
1150	289.17E-	242.19E-	904.16E-	820.15E-	258.13E-	96.6	30.37	99.5	237.1	0.5	56.05E-	23.33E-
1350	435.17E-	546.17E-	823.17E-	726.16E-	347.14E-	62.9	30.14	100	235.4	4.8	14.31E-	54.54E-
								Total	233.9	0.6		
9905Dc												
600	584.17E-	259.19E-	171.16E-	153.15E-	460.14E-	62.4	18.73	1	150.2	1.2	32.24E-	11.13E-
700	349.17E-	260.19E-	303.16E-	285.15E-	854.14E-	87.8	26.29	2.8	207.4	1.2	17.34E-	97.94E-
800	398.17E-	748.17E-	104.15E-	943.15E-	287.13E-	95.8	29.17	8.9	228.7	0.7	15.12E-	23.53E-
850	249.17E-	260.19E-	125.15E-	110.14E-	340.13E-	97.7	30.06	16.1	235.3	0.5	44.75E-	31.23E-
890	206.17E-	665.17E-	142.15E-	126.14E-	386.13E-	98.3	30.18	24.2	236.1	0.4	10.02E-	30.33E-
920	186.17E-	260.19E-	149.15E-	136.14E-	415.13E-	98.6	30.12	33	235.7	0.4	36.35E-	22.73E-
950	211.17E-	196.17E-	179.15E-	162.14E-	495.13E-	98.7	30.13	43.5	235.8	0.5	22.93E-	24.83E-
970	192.17E-	161.17E-	171.15E-	155.14E-	475.13E-	98.7	30.29	53.4	237	0.7	19.83E-	24.63E-
990	230.17E-	644.17E-	171.15E-	156.14E-	480.13E-	98.5	30.22	63.5	236.5	0.5	78.33E-	22.53E-
1010	248.17E-	260.19E-	172.15E-	156.14E-	479.13E-	98.4	30.26	73.6	236.7	0.5	31.85E-	25.23E-
1030	277.17E-	261.19E-	176.15E-	159.14E-	491.13E-	98.2	30.33	83.9	237.2	0.5	31.15E-	25.73E-
1050	266.17E-	261.19E-	144.15E-	131.14E-	406.13E-	98	30.41	92.3	237.8	0.6	37.95E-	24.43E-
1080	253.17E-	255.17E-	885.16E-	800.15E-	252.13E-	97	30.58	97.5	239.1	0.5	60.63E-	24.53E-
1110	194.17E-	261.19E-	368.16E-	328.15E-	106.13E-	94.5	30.53	99.6	238.7	0.8	15.14E-	26.93E-
1160	198.17E-	924.17E-	554.17E-	487.16E-	208.14E-	71.9	30.61	99.9	239.3	2.8	36.01E-	14.93E-
1350	420.17E-	109.15E-	238.17E-	131.16E-	163.14E-	24.6	30.84	100	241	17.8	15.81E+	52.73E-
								Total	234.8	0.6		
9905Ha												
600	319.17E-	249.19E-	125.16E-	110.15E-	256.14E-	63	14.69	0.9	119.4	2.9	43.24E-	19.83E-
700	273.17E-	205.17E-	275.16E-	243.15E-	571.14E-	85.8	20.12	2.9	161.6	0.8	16.02E-	26.13E-
800	355.17E-	250.19E-	700.16E-	607.15E-	151.13E-	92.9	23.04	7.8	183.9	0.5	78.15E-	34.63E-
850	368.17E-	250.19E-	669.16E-	572.15E-	155.13E-	92.9	25.21	12.4	200.3	0.8	83.05E-	38.23E-
890	201.17E-	250.19E-	735.16E-	643.15E-	178.13E-	96.6	26.76	17.6	211.9	0.5	73.95E-	33.43E-
920	167.17E-	250.19E-	766.16E-	673.15E-	192.13E-	97.3	27.81	23	219.7	0.6	70.65E-	32.73E-
950	237.17E-	250.19E-	109.15E-	961.15E-	284.13E-	97.4	28.76	30.8	226.8	0.6	49.55E-	31.63E-
970	179.17E-	250.19E-	117.15E-	103.14E-	308.13E-	98.2	29.3	39.2	230.8	0.5	46.05E-	31.03E-
990	199.17E-	250.19E-	124.15E-	110.14E-	331.13E-	98.1	29.44	48.1	231.9	0.4	43.25E-	30.13E-
1010	179.17E-	251.19E-	118.15E-	105.14E-	315.13E-	98.2	29.57	56.5	232.8	0.6	45.65E-	31.73E-
1030	248.17E-	251.19E-	110.15E-	968.15E-	294.13E-	97.4	29.56	64.4	232.7	0.5	49.25E-	30.93E-
1050	221.17E-	251.19E-	102.15E-	899.15E-	273.13E-	97.5	29.62	71.6	233.1	0.7	53.05E-	31.63E-
1080	235.17E-	538.17E-	112.15E-	997.15E-	302.13E-	97.6	29.57	79.7	232.8	0.5	10.22E-	28.53E-
1110	223.17E-	251.19E-	134.15E-	119.14E-	360.13E-	98.1	29.75	89.3	234.1	0.6	40.25E-	31.03E-
1160	236.17E-	251.19E-	116.15E-	103.14E-	311.13E-	97.7	29.55	97.6	232.6	0.5	46.45E-	28.93E-

Temp	Ar^{36}	Ar^{37}	Ar^{38}	Ar^{39}	Ar^{40}	% Radiogenic	$^{40}Ar^*/^{39}Ar$	Cum	Age	± 1s.d.	Ca/K	Cl/K
9905Ha Cont.												
1350	528.17E-	231.16E-	344.16E-	294.15E-	766.14E-	79.6	20.72	100	166.2	1.1	14.91E-	33.23E-
							Total		222.6	0.6		
9905Hb												
600	366.17E-	477.17E-	158.16E-	129.15E-	355.14E-	69.4	19.13	1.5	153.9	1.5	70.32E-	40.93E-
700	310.17E-	284.17E-	286.16E-	247.15E-	680.14E-	86.4	23.82	4.2	189.7	0.9	21.92E-	32.63E-
780	320.17E-	270.19E-	576.16E-	500.15E-	144.13E-	93.3	26.83	9.9	212.3	0.6	10.34E-	34.53E-
830	270.17E-	270.19E-	652.16E-	569.15E-	169.13E-	95.2	28.19	16.3	222.4	0.6	90.25E-	33.13E-
860	228.17E-	270.19E-	663.16E-	576.15E-	173.13E-	96	28.86	22.8	227.4	0.6	89.25E-	35.03E-
890	244.17E-	621.17E-	805.16E-	707.15E-	213.13E-	96.5	29.1	30.8	229.1	0.7	16.72E-	32.13E-
920	252.17E-	271.19E-	986.16E-	866.15E-	263.13E-	97.1	29.53	40.6	232.3	0.6	59.45E-	32.63E-
940	258.17E-	271.19E-	907.16E-	795.15E-	244.13E-	96.8	29.66	49.5	233.3	0.6	64.65E-	32.73E-
960	286.17E-	271.19E-	900.16E-	789.15E-	244.13E-	96.4	29.79	58.4	234.3	0.5	65.25E-	32.63E-
980	306.17E-	271.19E-	897.16E-	794.15E-	246.13E-	96.2	29.8	67.4	234.4	0.5	64.85E-	29.93E-
1000	309.17E-	271.19E-	885.16E-	782.15E-	243.13E-	96.2	29.88	76.2	234.9	0.5	65.85E-	30.23E-
1020	313.17E-	271.19E-	843.16E-	739.15E-	232.13E-	95.9	30.08	84.6	236.4	0.6	69.75E-	32.23E-
1050	330.17E-	361.19E-	699.16E-	614.15E-	193.13E-	94.9	29.83	91.5	234.5	0.8	11.24E-	31.43E-
1080	263.17E-	234.19E-	493.16E-	434.15E-	138.13E-	94.3	29.92	96.4	235.2	0.5	10.24E-	30.43E-
1140	260.17E-	442.17E-	299.16E-	266.15E-	870.14E-	91.1	29.77	99.4	234.1	0.8	31.62E-	25.23E-
1350	437.17E-	300.16E-	786.17E-	521.16E-	305.14E-	57.8	33.89	100	264.3	6.6	11.00E+	85.93E-
							Total		229.3	0.6		
9909a												
600	400.17E-	265.19E-	343.16E-	313.15E-	668.14E-	82.2	17.57	2.5	138.9	0.6	16.14E-	18.13E-
700	341.17E-	506.17E-	619.16E-	559.15E-	135.13E-	92.4	22.29	7	174.4	0.5	17.22E-	23.53E-
800	431.17E-	123.16E-	142.15E-	128.14E-	340.13E-	96.2	25.48	17.4	198	0.5	18.32E-	25.13E-
830	217.17E-	284.17E-	885.16E-	783.15E-	218.13E-	97	27.03	23.7	209.5	0.6	69.03E-	30.63E-
860	192.17E-	265.19E-	903.16E-	809.15E-	231.13E-	97.4	27.84	30.2	215.4	0.4	62.35E-	27.53E-
890	194.17E-	588.17E-	103.15E-	921.15E-	267.13E-	97.8	28.37	37.6	219.2	0.5	12.12E-	27.13E-
920	175.17E-	370.17E-	123.15E-	112.14E-	328.13E-	98.3	28.8	46.6	222.4	0.5	62.63E-	23.53E-
940	177.17E-	265.19E-	122.15E-	110.14E-	326.13E-	98.3	29.05	55.5	224.1	0.5	45.75E-	24.13E-
960	178.17E-	266.19E-	120.15E-	108.14E-	321.13E-	98.3	29.14	64.2	224.8	0.5	46.65E-	24.83E-
980	186.17E-	266.19E-	118.15E-	107.14E-	318.13E-	98.2	29.21	72.8	225.3	0.4	47.35E-	24.23E-
1000	196.17E-	266.19E-	113.15E-	103.14E-	309.13E-	98	29.27	81.2	225.7	0.5	48.85E-	22.63E-
1020	204.17E-	471.17E-	101.15E-	924.15E-	277.13E-	97.7	29.32	88.6	226.1	0.7	96.83E-	21.93E-
1050	201.17E-	266.19E-	846.16E-	769.15E-	233.13E-	97.4	29.42	94.8	226.9	0.6	65.75E-	23.33E-
1080	179.17E-	266.19E-	469.16E-	421.15E-	129.13E-	95.8	29.32	98.2	226.1	0.6	12.04E-	25.93E-
1140	207.17E-	314.17E-	136.16E-	118.15E-	373.14E-	83.5	26.35	99.1	204.5	2	50.42E-	28.13E-
1350	451.17E-	245.16E-	128.16E-	108.15E-	335.14E-	60.2	18.65	100	147.1	2.1	42.91E-	25.93E-
							Total		214.9	0.6		
9909b												
600	258.17E-	424.18E-	111.16E-	957.16E-	241.14E-	68.3	17.2	1	136.3	1.5	84.23E-	25.93E-
700	206.17E-	408.17E-	199.16E-	184.15E-	498.14E-	87.7	23.73	2.8	185.5	1	42.02E-	14.53E-
800	280.17E-	428.18E-	527.16E-	477.15E-	136.13E-	93.8	26.79	7.6	208.1	0.6	17.03E-	22.93E-
850	194.17E-	255.19E-	533.16E-	476.15E-	140.13E-	95.8	28.09	12.4	217.6	0.6	10.24E-	27.33E-
890	152.17E-	255.19E-	661.16E-	593.15E-	177.13E-	97.4	29.08	18.3	224.8	0.6	81.65E-	26.53E-
920	151.17E-	255.19E-	822.16E-	747.15E-	224.13E-	97.9	29.3	25.8	226.4	0.5	64.85E-	23.43E-
950	188.17E-	255.19E-	121.15E-	110.14E-	329.13E-	98.2	29.52	36.8	228	0.5	44.25E-	23.93E-
970	173.17E-	255.19E-	113.15E-	103.14E-	309.13E-	98.3	29.55	47.1	228.2	0.5	47.15E-	22.13E-
990	165.17E-	975.18E-	112.15E-	102.14E-	307.13E-	98.3	29.57	57.3	228.4	0.6	18.13E-	22.63E-
1010	175.17E-	255.19E-	102.15E-	930.15E-	281.13E-	98.1	29.63	66.7	228.8	0.7	52.25E-	21.73E-
1030	170.17E-	255.19E-	976.16E-	897.15E-	272.13E-	98.1	29.72	75.7	229.4	0.5	54.15E-	20.73E-
1050	192.17E-	256.19E-	908.16E-	825.15E-	250.13E-	97.6	29.61	83.9	228.7	0.7	58.95E-	23.53E-
1080	191.17E-	256.19E-	976.16E-	895.15E-	273.13E-	97.8	29.8	92.9	230.1	0.6	54.35E-	21.03E-
1110	167.17E-	256.19E-	618.16E-	559.15E-	173.13E-	97.1	30.03	98.5	231.7	0.5	87.05E-	24.73E-

Temp (˚C)	Ar^{36} (mol)	Ar37 (mol)	Ar38 (mol)	Ar39 (mol)	Ar40 (mol)	% Radiogenic 40Ar	40Ar*/39Ar	Cum 39Ar	Age (Ma)	± 1s.d. (Ma)	Ca/K	Cl/K
9909b Cont.												
1160	209.17E-	461.17E-	123.16E-	107.15E-	378.14E-	83.6	29.66	99.6	229	1.7	82.22E-	27.13E-
1350	379.17E-	754.17E-	599.17E-	439.16E-	211.14E-	46.9	22.6	100	177.1	5	32.71E-	49.53E-
								Total	225.1	0.6		
9909c												
600	258.17E-	251.19E-	149.16E-	132.15E-	319.14E-	75.9	18.39	1.2	145.2	0.9	36.34E-	22.73E-
700	313.17E-	252.19E-	278.16E-	255.15E-	656.14E-	85.8	22.09	3.5	173	1.4	18.84E-	17.03E-
800	370.17E-	252.19E-	707.16E-	631.15E-	175.13E-	93.6	25.89	9.3	201.2	0.6	75.75E-	26.53E-
850	206.17E-	252.19E-	699.16E-	623.15E-	179.13E-	96.5	27.64	15	214	0.6	76.85E-	28.23E-
890	208.17E-	252.19E-	817.16E-	729.15E-	214.13E-	97	28.46	21.7	220	0.6	65.75E-	28.23E-
920	165.17E-	252.19E-	941.16E-	850.15E-	253.13E-	98	29.14	29.4	225	0.6	56.35E-	25.43E-
950	196.17E-	386.17E-	124.15E-	113.14E-	336.13E-	98.2	29.23	39.7	225.6	0.5	64.83E-	22.03E-
970	205.17E-	252.19E-	122.15E-	111.14E-	333.13E-	98.1	29.43	49.9	227.1	0.4	43.25E-	22.83E-
990	185.17E-	252.19E-	120.15E-	110.14E-	332.13E-	98.3	29.53	60	227.7	0.5	43.45E-	20.43E-
1010	188.17E-	252.19E-	114.15E-	104.14E-	313.13E-	98.1	29.61	69.4	228.4	0.6	46.25E-	22.13E-
1030	190.17E-	410.17E-	107.15E-	981.15E-	297.13E-	98	29.71	78.4	229	0.7	79.53E-	20.73E-
1050	200.17E-	260.17E-	888.16E-	817.15E-	248.13E-	97.5	29.64	85.9	228.5	0.5	60.53E-	20.23E-
1080	190.17E-	253.19E-	945.16E-	868.15E-	265.13E-	97.8	29.83	93.8	229.9	0.6	55.35E-	20.63E-
1110	187.17E-	391.18E-	577.16E-	525.15E-	162.13E-	96.5	29.84	98.6	230	0.5	14.23E-	22.53E-
1160	215.17E-	189.16E-	111.16E-	981.16E-	342.14E-	81.4	28.36	99.5	219.2	2.1	36.61E-	21.73E-
1350	402.17E-	100.15E-	731.17E-	563.16E-	237.14E-	50.2	21.15	100	166	6.3	33.90E+	40.23E-
								Total	222.3	0.6		
9909d												
600	454.17E-	110.16E-	230.16E-	213.15E-	467.14E-	71.2	15.59	1.8	124.3	0.7	97.82E-	93.84E-
650	184.17E-	116.16E-	195.16E-	177.15E-	397.14E-	86.2	19.36	3.3	153.1	1.6	12.51E-	19.53E-
700	153.17E-	684.17E-	287.16E-	262.15E-	612.14E-	92.5	21.59	5.5	169.9	1.1	49.52E-	20.13E-
730	157.17E-	231.19E-	254.16E-	231.15E-	573.14E-	91.8	22.8	7.4	178.9	0.9	19.04E-	21.83E-
760	138.17E-	376.17E-	293.16E-	262.15E-	669.14E-	93.8	23.98	9.7	187.8	1	27.32E-	26.53E-
790	151.17E-	231.19E-	331.16E-	301.15E-	801.14E-	94.3	25.05	12.2	195.7	0.6	14.64E-	21.83E-
820	191.17E-	232.19E-	393.16E-	347.15E-	950.14E-	94	25.71	15.1	200.6	1.2	12.74E-	29.73E-
850	177.17E-	232.19E-	472.16E-	424.15E-	119.13E-	95.5	26.87	18.7	209.1	0.8	10.44E-	25.93E-
870	178.17E-	474.17E-	486.16E-	441.15E-	127.13E-	95.8	27.53	22.4	214	0.7	20.42E-	23.43E-
890	167.17E-	115.16E-	545.16E-	495.15E-	145.13E-	96.5	28.31	26.6	219.6	0.6	44.12E-	22.83E-
910	189.17E-	242.17E-	665.16E-	607.15E-	179.13E-	96.8	28.51	31.7	221.1	0.5	75.83E-	22.13E-
930	170.17E-	138.17E-	802.16E-	730.15E-	217.13E-	97.6	28.98	37.8	224.5	0.6	35.93E-	22.93E-
950	178.17E-	233.19E-	972.16E-	891.15E-	265.13E-	97.9	29.1	45.3	225.4	0.6	49.65E-	21.13E-
970	119.17E-	235.19E-	103.15E-	941.15E-	280.13E-	98.7	29.33	53.3	227.1	0.6	47.45E-	21.63E-
990	176.17E-	294.17E-	120.15E-	111.14E-	329.13E-	98.3	29.27	62.6	226.7	0.4	50.53E-	20.53E-
1010	183.17E-	235.19E-	118.15E-	108.14E-	322.13E-	98.2	29.44	71.6	227.9	0.5	41.65E-	22.73E-
1030	226.17E-	572.17E-	112.15E-	101.14E-	304.13E-	97.7	29.38	80.2	227.5	0.6	10.72E-	24.23E-
1060	227.17E-	230.17E-	115.15E-	105.14E-	315.13E-	97.8	29.37	89	227.4	0.5	41.63E-	22.03E-
1090	219.17E-	236.19E-	848.16E-	769.15E-	231.13E-	97.1	29.19	95.5	226	0.5	58.35E-	23.93E-
1140	279.17E-	406.17E-	299.16E-	273.15E-	805.14E-	89.7	26.4	97.8	205.7	1	28.22E-	18.53E-
1350	582.17E-	212.16E-	301.16E-	261.15E-	639.14E-	73	17.88	100	141.8	1.5	15.41E-	26.83E-
								Total	215.2	0.6		
9909e												
600	367.17E-	281.19E-	225.16E-	200.15E-	455.14E-	76	17.31	1.6	137.8	1	26.74E-	22.53E-
700	288.17E-	281.19E-	402.16E-	370.15E-	919.14E-	90.6	22.54	4.5	177.5	0.7	14.44E-	17.93E-
780	302.17E-	820.18E-	743.16E-	669.15E-	179.13E-	94.9	25.36	9.8	198.5	0.4	23.33E-	24.83E-
830	200.17E-	326.17E-	787.16E-	703.15E-	195.13E-	96.9	26.93	15.4	210	0.5	88.23E-	28.13E-
860	157.17E-	281.19E-	732.16E-	658.15E-	187.13E-	97.4	27.66	20.6	215.4	0.4	81.25E-	26.33E-
890	163.17E-	435.18E-	870.16E-	775.15E-	225.13E-	97.8	28.32	26.7	220.3	0.6	10.73E-	29.03E-
920	168.17E-	288.17E-	108.15E-	985.15E-	289.13E-	98.2	28.78	34.5	223.6	0.6	55.63E-	23.53E-

Temp	Ar^{36}	Ar^{37}	Ar^{38}	Ar^{39}	Ar^{40}	% Radiogenic	$^{40}Ar^*/^{39}Ar$	Cum	Age	± 1s.d.	Ca/K	Cl/K
9909e Cont.												
940	171.17E-	171.17E-	111.15E-	102.14E-	299.13E-	98.2	28.96	42.6	224.9	0.4	32.03E-	22.03E-
960	162.17E-	469.18E-	122.15E-	111.14E-	328.13E-	98.4	29.17	51.3	226.5	0.5	80.64E-	25.03E-
980	167.17E-	282.19E-	130.15E-	119.14E-	353.13E-	98.5	29.27	60.8	227.2	0.5	45.05E-	22.83E-
1000	177.17E-	282.19E-	136.15E-	123.14E-	366.13E-	98.5	29.4	70.5	228.2	0.6	43.65E-	25.43E-
1020	183.17E-	282.19E-	132.15E-	121.14E-	360.13E-	98.4	29.43	80	228.4	0.5	44.55E-	22.03E-
1050	174.17E-	159.17E-	133.15E-	122.14E-	366.13E-	98.5	29.59	89.7	229.5	0.6	24.83E-	22.13E-
1080	160.17E-	282.19E-	976.16E-	893.15E-	270.13E-	98.2	29.67	96.8	230.1	0.6	60.15E-	21.93E-
1140	174.17E-	434.17E-	393.16E-	359.15E-	111.13E-	95.3	29.51	99.6	229	0.6	23.02E-	21.03E-
1350	328.17E-	334.16E-	645.17E-	517.16E-	229.14E-	57.9	25.69	100	200.9	2.7	12.30E+	31.03E-
								Total	220.9	0.5		

argon release, up to temperatures of about 950°C. Not surprisingly, at higher temperatures the age spectra define plateau-like segments over large portions of gas release. At such temperatures it is expected that the argon released from the micas is effectively homogeneously released, due to dehydroxylation and eventual melting as the experiment progresses. In this respect, we believe that the plateau-like sections of the age spectra of these two samples are minimum estimates of the crystallization ages of these micas. In support of this argument we note that samples that exhibit more pronounced age gradients yield both lower total gas ages and lower plateau-like ages. On average, within this group the total gas ages are more than 4.5% lower than the plateau-like ages. In comparison, the total gas ages and the plateau-like ages are all lower than those exhibited by the other group of samples (ie., 9901, 9904, 9905A, 9905D). Mean plateau-like ages are 9905H = 233.5 ± 1.2 Ma, and 9909 = 227.3 ± 1.3 Ma, which are minimum estimates for the age of mica crystallization.

K-Ar data for eleven of the white mica concentrates (Table 1) indicates close agreement with $^{40}Ar/^{39}Ar$ total gas ages (Figure 2). This consistency effectively rules out the possibility of recoil loss of ^{39}Ar related to neutron irradiation associated with $^{40}Ar/^{39}Ar$ dating. Moreover, the spectra are not indicative of recoil loss patterns, which would yield elevated ages in the initial release. On average the K-Ar ages are slightly younger than the associated $^{40}Ar/^{39}Ar$ total gas ages, which we believe is an artifact of the data reduction, as $^{40}Ar/^{39}Ar$ dating relies on a secondary standard which we have chosen, by preference, to be slightly older than the original published age (cf., McDougall and Roksandic, 1974; Renne *et al.*, 1998; see also notes for Tables 1 and 2). We draw attention to the high K contents of these concentrates. For such fine-grained micas we are unaware of a study that has attained such high purities; nevertheless there are significant contaminants, as indicated in the next section. Note also that there is a rough correlation between the lower K contents in Table 2 and lower ages, suggesting that the contaminants may play a role in the determination of age (see below).

Rb-Sr analysis of three of the white mica concentrates has yielded information that has been used to estimate ages based on one-point isochrones. Although potentially misleading, we have chosen (blindly, in fact) to estimate ages using an initial 87Sr/86Sr of 0.710, a not unrealistic value for such rocks. The results indicate excellent agreement with K-Ar and $^{40}Ar/^{39}Ar$ ages (Table 2), an outcome that has a significant bearing on our interpretation of the $^{40}Ar/^{39}Ar$ results, below.

XRD Analysis of Zhangbaling Micas

We attempted XRD analysis of the white mica concentrates to try and understand the cause of the strong age gradients, particularly to see if some contaminating phases could be responsible, or if a mixture of micas with different stacking orders gave contrasting $^{40}Ar/^{39}Ar$ spectral patterns. These avenues of inquiry were both answered by the XRD results. All of the white mica concentrates gave XRD patterns identical to muscovite with a 2M1 structure. Contaminating phases in concentrates 9901a, 9904c, 9905Ac, 9905Dc, 9905Hb, and 9909a are minor amounts of quartz and albite, with the notable addition of hematite in concentrate 9909a.

Inspection of Zhangbaling Micas

In the quest to interpret the $^{40}Ar/^{39}Ar$ age spectra I elected to take a closer look at the concentrates to see if I could identify some correlation between spectral pattern and concentrate characteristics. A review of the concentrates under oil with a petrographic microscope indicates that the curved spectra are associated with white micas that have abundant quartz and albite inclusions and/or hematite inclusions and intergrowths.

Figure 4 shows photomicrographs of each white mica concentrates in oil. Instead of showing a statistically significant number of grains at low magnification (100's) we thought it useful to use higher magnification. In showing a limited number of grains in Figure 4 we had to be careful to select a group of grains considered characteristic of the concentrate as a whole.

Several conclusions can be drawn by comparing the photomicrographs in Figure 4 with the age spectra in Figure 2. Concentrates from samples 9905H and 9909 are heavily included and/or intergrown with quartz, albite, and hematite, right down to the smallest grain size fractions. All of the age spectra for these samples show strong age gradients.

In contrast, most of the concentrates from samples 9901, 9904, 9905A and 9905D contain must lower levels of inclusions and intergrowths. In this group, a notable

exception is concentrate 9904b, which contains much more contamination than either 9904a or 9904c, and exhibits strong age gradients in the age spectrum. Inclusions in the five concentrates from samples 9901 and 9905A are also prevalent, but not at the levels seen in samples 9905H and 9909, and the opaque minerals tend to be more isolated or occur as separate fragments. Concentrates from sample 9905D are the cleanest of all.

Given that XRD analysis has failed to identify opaque minerals in all cases except sample 9909, it was hypothesized that the opaque minerals form only a very small volume fraction of the concentrates despite their presentation in Figure 4. It seemed likely that most of the opaque inclusions could be thin blades grown along the cleavages of the micas, thus the density close to mica rather than hematite. Examination of grains cut parallel to the c-axis has confirmed this.

In summary, there is a broad correlation between the level of contamination of the white micas by inclusions and intergrowths with quartz, albite and hematite, and the associated age spectrum patterns. Age spectra that show strong age gradients exhibit the highest concentrations of intergrowths and inclusions.

Interpretation of Zhangbaling Results

The rising character of the 40Ar/^{39}Ar age spectra for samples 9905H and 9909, as well as for concentrate 9904b, are indicative of either pronounced intragrain age gradients within a homogeneous population of grains, or a population of grains with a wide range of individual grain ages. No correlation between age and grain (sieve) size is apparent, however, as would be expected for intragrain age gradients produced by slow cooling (e.g., Goodwin and Renne, 1991). In addition, early in this study we ruled out the possibility of a wide range of single grain ages, as a product of a series of deformations, due to the homogeneity of the microstructures of the rocks. So what is the cause of the pronounced age gradients?

The key to understanding and interpreting the age spectra is the petrographic observations. The reason there is no correlation between grain size and age is that the mesh size of the concentrates is not a true representation of the effective diffusion dimension for argon in the micas. The micas in samples 9905H and 9909, and concentrate 9904b, are so dissected by inclusions and intergrowths that the notion of an effective diffusion dimension is inappropriate. The microstructures seen in Figure 4 suggest that there are a wide range of effective diffusion dimensions in the micas. The white mica concentrates with the widest range of effective diffusion dimension, those with the highest density of inclusions and intergrowths, have clearly experienced argon loss subsequent to their formation, at a time less than or equal to the youngest age steps. The above argument indicates that the process responsible for the strong age gradients in concentrates from samples 9905H and 9909 is loss of ^{40}Ar via thermally activated diffusion, deformation being effectively ruled out as a resetting process.

Considering the metamorphic grade and microstructure of the samples, and previous experience in the ^{40}Ar/^{39}Ar dating of such materials (Dunlap *et al.*, 1991, Dunlap, 1997, Dunlap *et al.*, 1997), I interpret the plateau-like sections of age spectra for concentrates from samples 9901, 9904, 9905A and 9905D as ages of mica formation, or crystallization ages. Further support and confirmation of this conclusion is provided by the Rb-Sr data for concentrates 9904a, 9905Ab, and 9905Dc, which all give ages within error or slightly younger than the associated ^{40}Ar/^{39}Ar ages. Given that the closure temperature for the Rb-Sr system in white micas is considered to be of the order of 500°C, whereas that of the argon system is ~350°C (Hames and Bowring, 1996), we can effectively rule out lowering of the argon ages of these concentrates through diffusive loss of ^{40}Ar. The plateau-like ages for samples 9901, 9904, 9905A and 9905D provide ages of the cessation of deformation (cf. Dunlap, 1997) in the Zhangbaling metamorphic belt between 235.4 Ma and 238.5 Ma.

The cause of the strong age gradients in the age spectra for samples 9909 and 9905H is likely to be reheating or slow cooling. Given the proximity of these samples to a large Cretaceous intrusion (Zhang *et al.*, submitted) it is clear that the finely dissected microstructure of the micas in these samples has allowed argon loss via thermally activated diffusion at lower temperatures than would normally be expected for white micas. The plateau-like ages for samples 9909 and 9905H should be considered intermediate between crystallization and cooling ages, thus lacking any real geochronological significance.

Forlandsundet Micas - Background

The Western Spitsbergen fold-and-thrust belt has been attributed to oblique convergence along an intracontinental transform between the northwestern Barents Shelf and Greenland (Harland, 1969). Plate reconstructions as well as structural, thermochronologic, and stratigraphic evidence suggest thrust belt deformation was as young as Late Cretaceous (cf. Blythe and Kleinspehn, 1998). The studied micas are from the Paleogene Forlandsundet Basin, western Spitzbergen, which is flanked by uplifted Caledonian (early Paleozoic) basement on all sides. The Forlandsundet basin is one of five onshore Paleogene basins in Svalbard attributed to deformation along the intracontinental transform. Shifting Late Cretaceous-Paleogene relative plate motions led to phases of oblique extension, to which sedimentation in the Forlandsundet basin has been correlated (e.g., Müller and Spielhagen, 1990).

The basin fill displays multiple open to tight folds and foliated zones associated with thrusting and strike-slip faulting. The metamorphism associated with the deformation of the basin was anchizonal, involving temperatures much lower than would be expected to result in argon loss from white micas (below ~250°C). However, the micas do appear to have been affected by both deformation and by extensive growth of iron oxide inclusions inside them (Figure 5), and the dating was undertaken to see if any Tertiary resetting of the micas had occurred (cf. Dallmayer, 1989). It is not clear when the inclusions grew, but it is likely that they grew during either

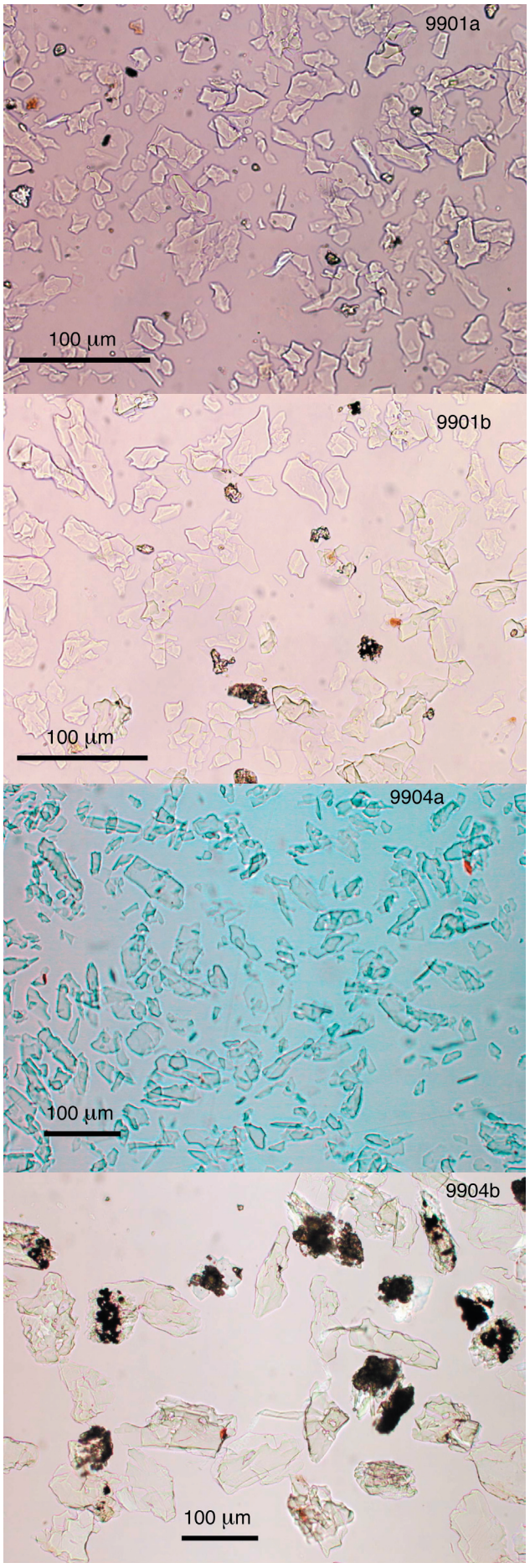
9901a
100 µm
9901b
100 µm
9904a
100 µm
9904b
100 µm

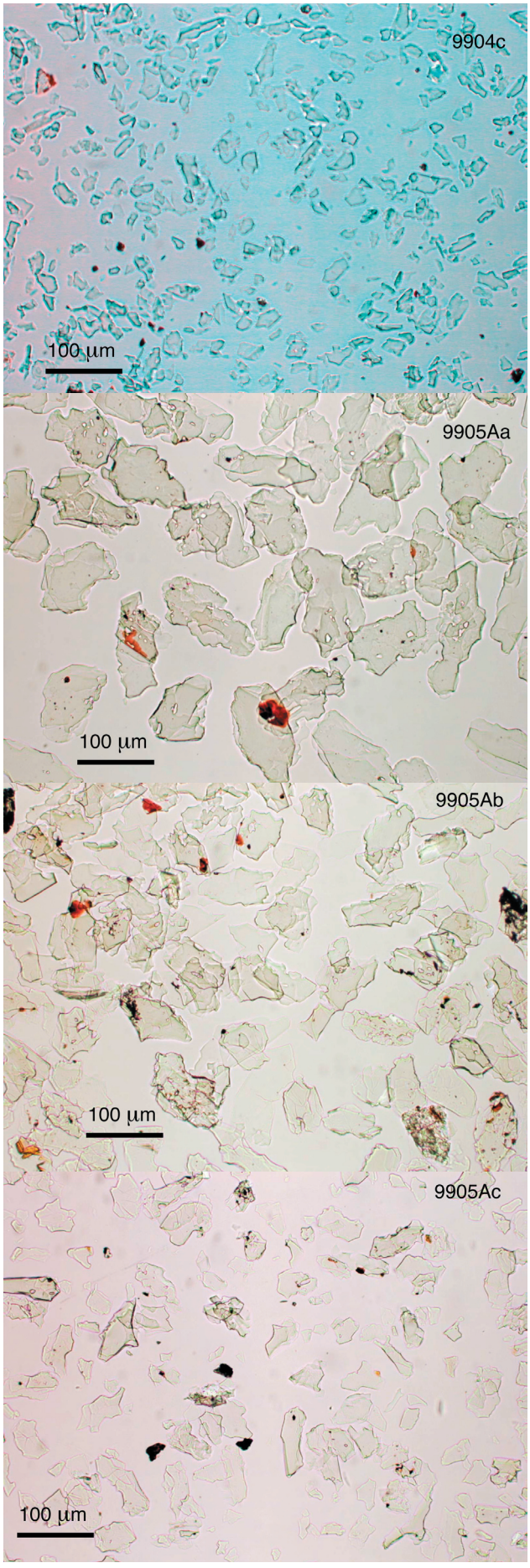
9904c
100 µm
9905Aa
100 µm
9905Ab
100 µm
9905Ac
100 µm

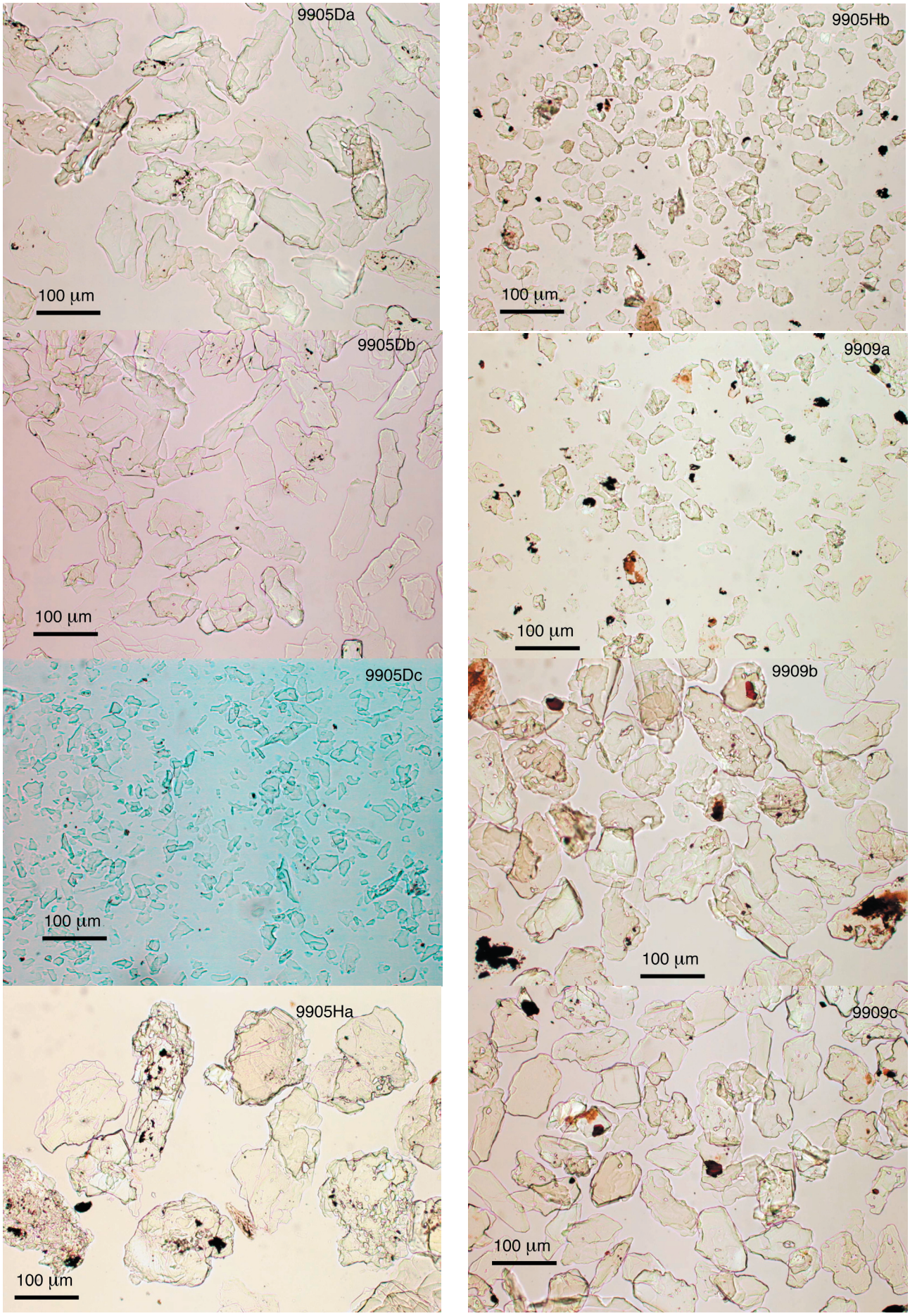
9905Da
100 µm
9905Hb
100 µm
9905Db
100 µm
9909a
100 µm
9905Dc
100 µm
9909b
100 µm
9905Ha
100 µm
9909c
100 µm

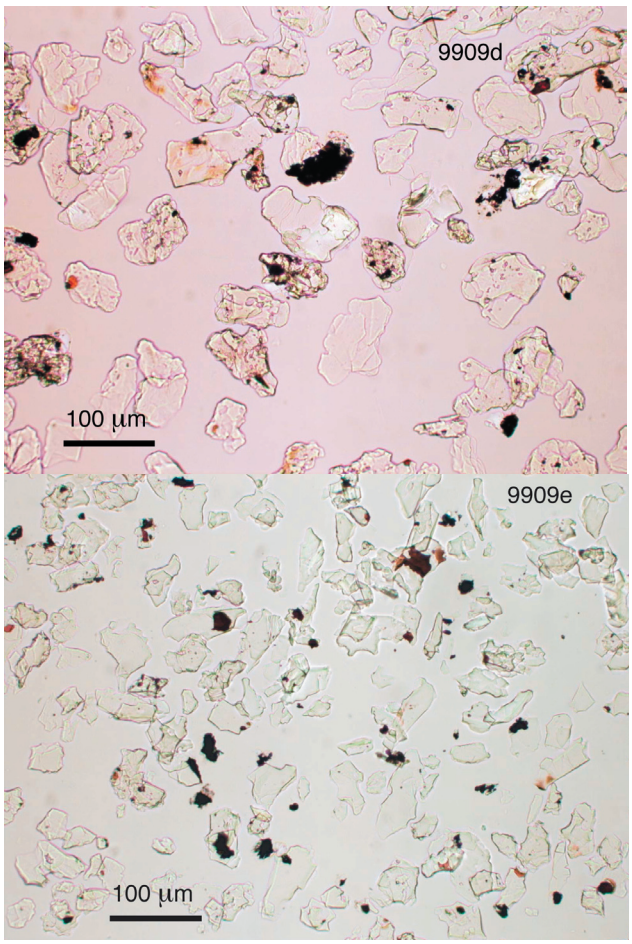

Figure 4: Photomicrographs of white mica concentrates from the Zhangbaling rocks in oil.

the Paleogene anchizonal metamorphism, or during thrust belt development in the Cretaceous.

The source of the sediments is from the adjacent Caledonian metamorphic basement, which is characterized by micas that yield $^{40}Ar/^{39}Ar$ ages between 410-480 Ma (Dallmeyer, 1989; Dallmeyer *et al.*, 1990). According to Blythe and Kleispehn (1998) maximum temperatures reached in the basin were not high enough to reset the fission tracks in detrital zircons. Nine of ten zircons analysed yielded Caledonian or Proterozoic ages. Thus, it appears from independent thermal information that the sediments never reached temperatures greater than about 220°C since Caledonian time.

Analysis of Forlandsundet Micas

The white micas were concentrated from the sedimentary rock by procedures nearly identical to those outlined for the Zhangbaling micas. A range of grain size fractions were separated, but centrifuged density fractions other than 2.75-2.96 g/cc were not prepared. It was noted before dating that all of the white mica concentrates have a distinctly bimodal character, with about half the grains being clear, clean single crystals, and the other half being heavily included crystals.

Figure 6 is a photomicrograph of concentrate 444A (38- 53 micron) in oil, and it can be considered representative of all the concentrates. Despite the apparent homogeneity in the studied concentrates, however, the proportion of included grains varies from about 20% to about 90%. The inclusion population in all concentrates is composed of iron oxides and a variety of inclusions with rod shapes that appear to be apatite and rutile, although their compositions have not been measured. The inclusion population does not appear to contain feldspars or any high-K phases. Despite some reservations about the purity of the micas it was decided to proceed with the dating study, with hopes of getting some information about resetting of the isotopic system in Cretaceous or Tertiary time.

The results, shown in Figure 3, show dramatic age gradients that were very much unexpected. The strong age gradients are not consistent with the known thermal history of the sediments, or of the adjacent metamorphic basment. If the closure temperature of the white micas is about ~350°C, for such grain sizes, it would be unusual to see ages younger than about 410-480 Ma, the ages characteristic of the micas in the adjacent basement rocks.

The data is remarkably internally consistent in terms of the range of ages recorded by the micas. The initial step for all the micas except one is Cretaceous in age, with subsequent steps rising continuously in a staircase pattern to Paleozoic or older maximum ages between 360 Ma and 597 Ma. Curiously, the mean age of the first step in each spectrum is well defined at 81 ±3 Ma (1 sigma error on population). There is not, in general, any good correlation between bulk age and grain size, as for example the size fractions of concentrates 444A and 232. However, two very fine concentrates of sample 108 (<2 m, 2-6 m), and one coarser fraction (10-38 m), do show a trend toward younger bulk age with finer grain size. It seems likely that grains with diffusion dimensions less than about 3 microns were susceptible to diffusion loss of argon, but that coarser grains were not.

Perhaps the most interesting correlation is that the concentrates with the highest percentage of included grains tend to yield the youngest bulk ages. For example, of the four concentrates of 444A the larger size fractions have progressively more included grains, but it is the smallest fraction (10-38 m), the one with the more clean grains, that yields the highest bulk age. Similarly, concentrates 586 (10-38) and 236 (10-38) have high percentages of included grains and they yield the youngest bulk ages (finer concentrates of 108 excluded). Thus, there is a strong indication that the proportion of included grains has a control on bulk age.

The K/Ca patterns for the micas are all hump shaped, starting with ratios that are low (<1 to about 50) in the early gas release and rising to peak values typically between 50- 200 in the middle of gas release. During melting the K/Ca then falls dramatically back to much lower values (while the age continues to climb). Dallmeyer *et al.* (1990) has demonstrated that the white micas in the nearby basement rocks are either muscovite or paragonite, and that they contain little or no Ca. It seems likely that the source of the Ca may be apatite inclusions, but no firm conclusion can be made at this time without further investigation.

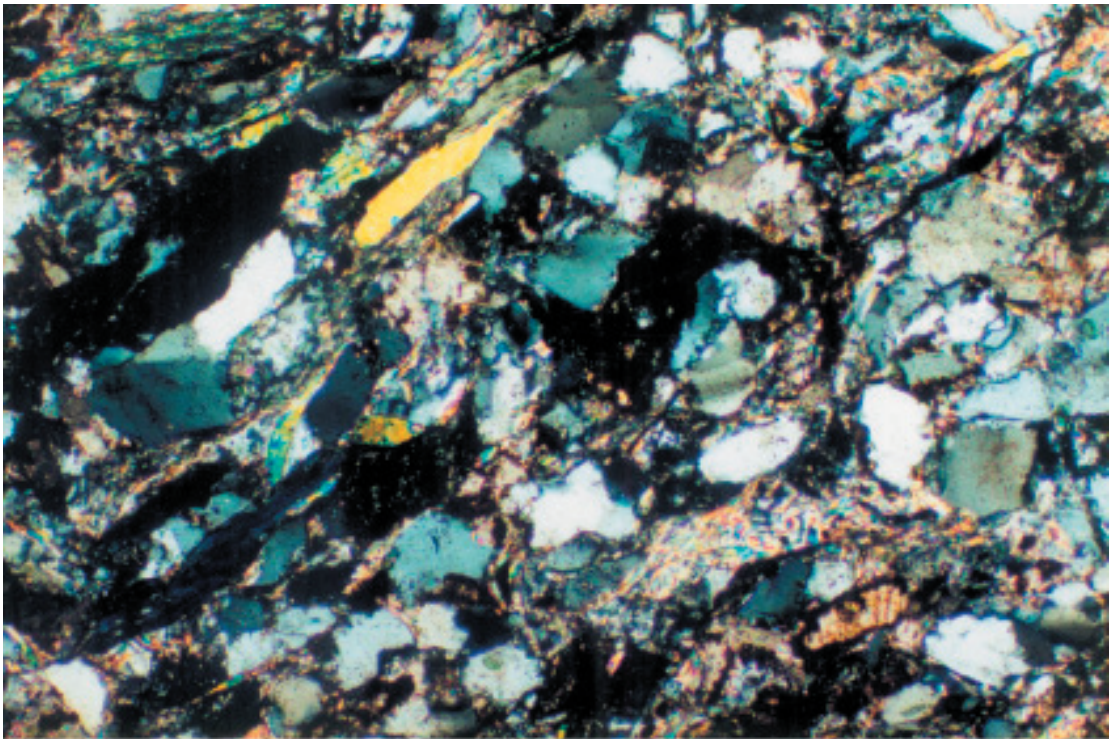

Figure 5: Cross-polars photomicrograph of sedimentary rock 576 from the Forlandsundet Basin. Long dimension of photo is ~1.5 mm.

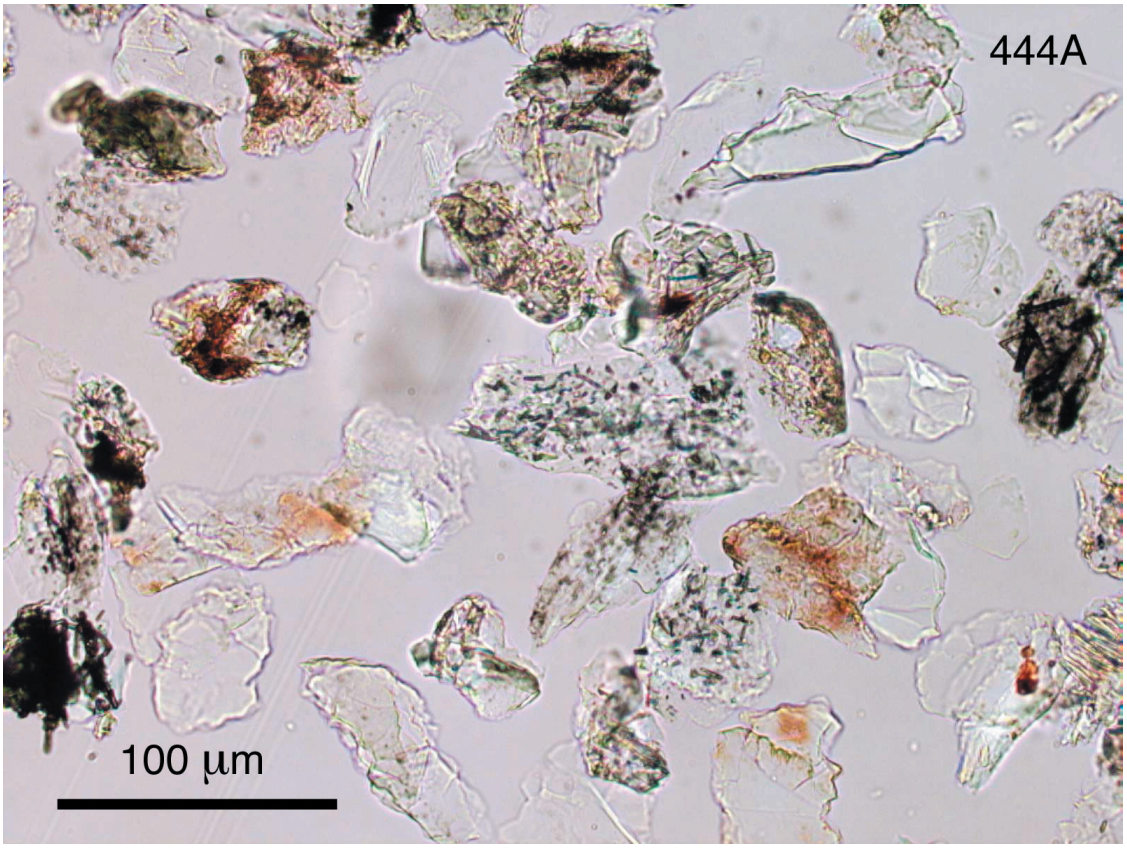

Figure 6: Photomicrograph of white mica concentrate 444A, 38-53 micron fraction, in oil. All of the white mica concentrates from the Forlandsundet rocks look similar to this sample, except for wide variations in the proportion of included grains.

Interpretation of Forlandsundet Micas

Given the thermal histories of both the Forlandsundet Basin sediments and the adjacent Caledonian metamorphic basement, the age spectra are difficult to explain in terms of tectonothermally driven argon loss. Even though the samples were taken from different parts of the basin, and different stratigraphic units, the fact that the samples are a sedimentary mixture of grains from the surrounding basement would seem to explain the consist shape of the spectra and the similar initial age steps.

But why the pronounced age gradients? Micas from the adjacent basement do not show such a pronounced younging in the initial gas release (Dallmeyer *et al*., 1990). Given the high grade of the basement rocks it is reasonable to assume that Dallmeyer *et al*. (1990) dated much coarser grained micas, as these are much easier to concentrate and clean. Assuming this is true, the pronounced younging of the micas in the present study must be a function of their post-erosional history.

The white micas do not appear to be substantially recrystallised. The most obvious choice for the cause of younging is thermally activated, diffusive loss of argon. The only correlation between grain size fraction and age, however, is indicated by the concentrates that have diffusion radii or 3 microns or less. But, the sieve size fraction of the coarser white micas is, as in the Zhangbaling study, not a true indication of effective diffusion dimension, due to the preponderance of inclusions in many grains. Thus, coarse, clean grains should have closure temperatures of ~350- 400 °C, but grains riddled with inclusions that provide channels for gas release will obviously have lower closure temperatures.

The preferred interpretation is that the pronounced younging in the age spectra is caused by diffusive loss of argon from the heavily included grains, due to the breakdown of their domain structure by the inclusions. Paleozoic ages are still reached in the later stages of gas release because the clean single crystals in the concentrates still retain the metamorphic cooling age of the adjacent basement. If the inclusions reduce the effective diffusion dimension of the white micas to the micron scale the closure temperature is likely to be reduced to ~250°C. This is still slightly higher than temperatures reached during the deformation of the Forlandsundet Basin. In this respect it is curious that the youngest age steps for these micas are almost all Cretaceous rather than Paleogene. No firm conclusion can be made regarding the timing of outgassing, due to the mixing of gas from both included and clean grains in the earliest gas release. But what seems certain is that the preponderance of the included grains is the cause of the pronounced age gradients.

DISCUSSION AND CONCLUSIONS

Two case studies have been presented, one of micas from the Zhangbaling schist and another of micas from the Forlandsundet Basin. Both studies yield strong evidence that pronounced age gradients in the age spectra of extremely fine grained white micas are controlled by low-K inclusions. There is a strong correlation between the frequency of the inclusions and lower bulk ages of the micas. In both cases the lowering of the age is a product of diffusive loss of argon, preferentially from the most included grains, due to a dramatic decrease in the effective diffusion dimension. This indicates that the inclusion grain boundaries act as either fast pathways for intragrain diffusion, within the micas, and/or open channels for argon loss if the inclusions intersect the mica grain edge.

A most interesting finding is that the step heating process does not homogenize the gas release, providing false plateaus, to the extent suggested by Hodges *et al*. (1993). This is probably due to the wide range in effective grain sizes, allowing gas to be released from the most included grains (and the inclusions; ^{37}Ar) in the early steps, likely by a combination of diffusion and breakdown by dehydroxylation. Later gas release is dominated by the clean white mica single crystals.

The regional thermal history of both case study areas indicates that argon loss took place at temperatures below the commonly cited closure temperature for white micas (~350-400°C). This provides confirmation that the bulk closure temperature of the heavily included grains is considerably lower, possibly around 250°C.

In the case of the Zhangbaling micas, the plateau-like ages of the clean concentrates that contain few inclusions are flat for ~80-95% of gas release, and the data yields crystallization ages related to the cessation of deformation, rather than cooling ages, as indicated by the Rb-Sr data. Concentrates with a larger proportion of included grains yield strongly curved age spectra and lower plateau-like ages, due to diffusive loss of argon subsequent to crystallization of the grains. These conclusions are supported by the geological history, which indicates a Cretaceous reheating event.

In the case of the Forlandsundet micas, all concentrates contain large numbers of included grains, and none of the age spectra yield plateau-like sections over large portions of gas release. The range of ages expressed in the spectra are a product of multiple length scales for diffusive loss of argon (i.e., variable closure across individual mica grains). The early gas release is dominated by the included grains, and the inclusions (^{37}Ar), whereas the later release is dominated by clean grains of early Paleozoic age. The age and temperature of outgassing of the included grains is likely to be Late Cretaceous, across a temperature window around 250°C. However, Paleogene outgassing cannot be ruled out.

This work has implications for studies that employ $^{40}Ar/^{39}Ar$ dating of white micas, particularly for fine grained rocks. If heavily included grains form a significant fraction of a white mica concentrate (>~a few %), and the thermal history of the rock was complex (through ~200-350°C), it is likely that the age spectrum will exhibit pronounced age gradients, regardless of the homogenizing effects of furnace step heating. For micas extracted from very fine grained rocks this can be a serious problem, because included grains are difficult to filter out with conventional mineral separation techniques. Nevertheless, it is possible in many cases to select greenschist facies rocks that contain few included micas (cf. Dunlap, 1997). Greenschist facies tectonites with visible opaque minerals

should be avoided when selecting samples for the dating of fine grained white micas. One advantage realised here is that included grains may provide a test for low temperature (~200-250°C) thermal pulses that would not otherwise be manifested in the K-Ar system of clean single crystals of white mica. This approach may be useful in cases where K-feldspars are not available.

REFERENCES

Beyssac, O., Goffe, B., Chopin, C., and Rouzaud, J.N., 2002, Raman spectra of carbonaceous material in metasediments: a new geothermometer: Journal of Metamorphic Geology, v. 20 (9), p. 859-871.

Blythe, A.E., and Kleinspehn, K.L., 1998, Tectonically versus climatically driven Cenozoic exhumation of the Eurasian plate margin, Svalbard: Fission track analysis: Tectonics, v. 17, p. 621-639.

Cebula, G.T., Kunk, M.J., Mehnert, H.H., Naeser, C.W., Obradovich, J.D. and Sutter, J.F., The Fish Canyon Tuff, a potential standard for the $^{40}Ar/^{39}Ar$ and fission track dating methods, Terra Cognita, 6, 139, 1985.

Chopin, C. and Maluski, H., 1980, ^{40}Ar-^{39}Ar dating of high pressure metamorphic micas from the Gran Paradiso area (western Alps): Evidence against the blocking temperature concept: Contribution to Mineralogy and Petrology, v. 74, p. 109-122.

Cliff, R.A., 1985, Isotopic dating in metamorphic belts: Journal of the Geological Society of London, v. 142, p. 97-110.

Dallmeyer, R.D., Partial thermal resetting of $^{40}Ar/^{39}Ar$ mineral ages in western Spitsbergen Svalbard: Possible evidence for Tertiary metamorphism., Geological Magazine, 126, 587-593, 1989.

Dallmeyer, R.D., J.J. Peucat, T. Hirajima, and Y. Ohta, Tectonothermal chronology within a blueschist-eclogite complex, west-central Spitsbergen, Svalbard: Evidence from $^{40}Ar/^{39}Ar$ and Rb-Sr mineral ages, Lithos, 24, 1-14, 1990.

Desmons, J., Hunziker, J.C., and Delaloye, M., 1982, Unconvincing evidence against the blocking temperature concept: Contributions to Mineralogy and Petrology, v. 80, p. 386-390.

Dodson, M.H., 1973, Closure temperature in cooling geochronological and petrological systems: Contribution of Mineralogy and Petrology, v. 40, p. 259-274.

Dunlap W.J., and Teyssier, C., 1995, Paleozoic deformation and isotopic disturbance in the southeastern Arunta Block, central Australia: Precambrian Research, Volume on Australasian Tectonics, v. 71, p. 229-250.

Dunlap, W.J., 1997, Neocrystallization or Cooling?: $^{40}Ar/^{39}Ar$ ages of white micas from low grade mylonites. Chemical Geology (isotope geoscience section): v. 143, p. 181-203.

Dunlap, W.J., 1998, comment: The tectonic significance of a porphyroblastic blueschist facies overprint during Alpine orogenesis: Sifnos, Aegean Sea, Greece: by G. S. Lister and A. Raouzaios: Journal of Structural Geology, v. 20 p. 819-821.

Dunlap, W.J., 2000, Nature's diffusion experiment: The cooling-rate cooling-age correlation: Geology, v. 28, p. 139-142

Dunlap, W.J., Teyssier, C., McDougall, I., and Baldwin, S., 1991, Ages of deformation from $^{40}Ar/^{39}Ar$ dating of white micas: Geology, v. 19, p. 1213-1216.

Dunlap, W.J., Teyssier, C., McDougall, I. and Baldwin, S.L., 1995, Thermal and structural evolution of the intracratonic Arltunga Nappe Complex, central Australia: Tectonics, v. 14, p. 1182-1204.

Dunlap, W.J., Hirth, G., and Teyssier, C., 1997, Thermomechanical evolution of a ductile duplex. Tectonics, v. 16, p. 983-1000.

Dunlap, W.J., and Kronenburg, A., 2001, Argon loss during deformation of micas: Constraints from experimental deformation studies: Contributions to Mineralogy and Petrology, v. 141(2), p. 174-181.

Goodwin, L.B., and Renne, P.R., 1991, Effects of progressive mylonitization on Ar retention in biotites from the Santa Rosa Mylonite Zone, California, and thermochronologic implications: Contributions to Mineralogy and Petrology, v. 108, p. 283-297.

Hames, W.E. and Bowring, S.A., 1994, An empirical evalutation of the argon diffusion geometry in muscovite: Earth and Planetary Science Letters, v. 124, p. 161-167.

Harland, W.B., Contribution of Spitsbergen to understanding of tectonic evolution of North Atlantic Region, in North Atlantic - Geology and Continental Drift, edited by M. Kay, American Association Petroleum Geologists Memoir 12, 817-851, 1969.

Harrison, T.M., Duncan, I., and McDougall, I., 1985, Diffusion of ^{40}Ar in biotite: Temperature, pressure and compositional effects: Geochimica et Cosmochimica Acta, v. 49, p. 2461-2468.

Hirth, G., and Tullis, J., 1992, Dislocation creep regimes in quartz aggregates: Journal of Structural Geology, v. 14, p. 145-160.

Hodges, K.V., Hames, W.E., and Bowring, S.A., 1993, $^{40}Ar/^{39}Ar$ age gradients in micas from a high-temperature-low-pressure metamorphic terrain: Evidence for very slow cooling and implications for the interpretation of age spectra: Geology, v. 22, p. 55-58.

Kligfield, R., Hunziker, J., Dallmeyer, R.D., and Schamel, S., 1986, Dating of deformation phases using K-Ar and $^{40}Ar/^{39}Ar$ techniques: results from the Northern Appenines: Journal of Structural Geology, v. 8, p. 781-798.

Kramar, N., Cosca, M.A., Hunziker, J.C. (2001) Distribution and significance of radiogenic argon in deformed muscovite: evidence from in-situ UV-laser ablation $^{40}Ar/^{39}Ar$ geochronology. Earth. Planet. Sci. Lett. 192, 377-388.

Lee, J.K.W., Multipath diffusion in geochronology: Contributions to Mineralogy and Petrology, v. 120, p. 60-82.

Lister, G.S., and Baldwin, S.L. (1996) Modelling the effect of arbitrary P-T-t histories on argon diffusion in minerals using the MacArgon program for the Apple Macintosh: Tectonophysics, v. 253, p. 83-109.

Lister, G.S. & Raouzaios, A. 1996. The tectonic significance of a porphyroblastic blueschist facies overprint during Alpine orogenesis: Sifnos, Aegean Sea, Greece. J. Struct. Geol., 18, 1417-1435.

Markley, M., Teyssier, C., and Cosca, M. (2002) The relation between grain size and $^{40}Ar/^{39}Ar$ age for Alpine white mica from the Siviez-Mischabel Nappe, Switzerland. J. Struct. Geol. (in press).

McDougall, I., and Harrison, T.M., Geochronology and Thermochronology by the $^{40}Ar/^{39}Ar$ Method: New York, Oxford University Press, second edition, 269 p., 1999.

McDougall, I., and Roksandic, Z., 1974, Total fusion $^{40}Ar/^{39}Ar$ ages using HIFAR reactor: Geological Society of Australia Journal, v. 21, p. 81-89.

Mulch, A., Cosca, M.A., and Handy, M.R. (2002) In situ UV-laser $^{40}Ar/^{39}Ar$ geochronology of a micaceous mylonite: an example of defect-enhanced argon loss. Contrib Mineral Petrol 142, 738-752.

Müller, R.D., and R.F. Spielhagen, Evolution of the Central Tertiary Basin of Spitsbergen: Towards a synthesis of sediment and plate tectonic history, PPP, 80, 153-172, 1990.

Phillips, D. and Onstott, T.C. (1988). Argon isotopic zoning in mantle phlogopite. Geology, 16, 542-546.

Renne, P.R., Swisher, C.C., Deino, A.L., Karner, D.B., Owens, T.L., and DePaolo, D.J., 1998, Intercalibration of standards, absolute ages and uncertainties in $^{40}Ar/^{39}Ar$ dating: Chemical Geology (Isotope Geoscience Section), v. 145, p. 117-152.

Steiger, R., and Jäger, E., Subcommission on geochronology: Convention on the use of decay constants in geo- and cosmochronology, Earth and Planetary Science Letters, 36, 359-362, 1977.

Xu, J., Zhu, G., Tong, W., Cui, K., and Liu, Q., 1987, Formation and evolution of the Tancheng-Lujiang wrench system: a major shear system to the northwest of the Pacific Ocean. Tectonophysics, 134:273-310.

Wijbrans, J. and McDougall, I., 1986, $^{40}Ar/^{39}Ar$ dating of white micas fromm an Alpine high-pressure metamorphic belt on Naxos (Greece): The resetting of the argon isotopic system: Contributions to Mineralogy and Petrology, v. 93, p. 187-194.

Zingg, A., and Hunziker, J.C., 1990, The age of movements along the Insubric Line west of Locarno (northern Italy and southern Switzerland): Eclogae Helvetica., v. 83, p. 629-644.

APPENDIX: ANALYTICAL PROCEDURE

Isotopic analyses were performed at both the University of California, Los Angeles, Department of Earth and Space Sciences (UCLA) and The Australian National University, Research School of Earth Sciences (ANU).

Petrographic examination of the white micas suggests that the resultant grain-size distributions are skewed toward the coarser end of the sieve fractions. This result is expected because the micas approximate ellipsoidal disks, with the intermediate dimension within the cleavage allowing passage of grains through the sieve openings, despite their being longer in another dimension.

The samples were weighed, packed in tin or Al foil and stacked in quartz tubes for irradiation. The irradiation tube packed at ANU utilized K-glass and CaF2 to monitor production ratios associated with interfering reactions, cadmium shielding to control the thermal to fast neutron-flux ratio (McDougall and Harrison, 1999), and the fluence monitor GA 1550 biotite (98.79 Ma, McDougall and Roksandic, 1974; Renne *et al*., 1998). Irradiation for sample done at ANU was conducted at the HIFAR reactor, Lucas Heights, Australia, thanks to the Australian Science and Technology Organisation and the Australian Institute of Nuclear Science and Engineering. The irradiation tube packed at UCLA utilized K2SO4 and CaF2 salts and the fluence monitor Fish Canyon Sanidine (27.8 Ma; Cebula *et al*., 1985). This irradiation was carried out at the Ford reactor at the University of Michigan for 45 hours in site L67.

During the course of the step-heating experiments, temperatures of extraction were monitored by a thermocouple inserted into the base of a tantalum crucible and maintained at the specified temperatures through feedback to a furnace controller. No liner was used inside the crucibles. Based on the signal from the thermocouple, the precision of the temperature reading is expected to be ±1°C; however, the absolute temperature experienced by the samples may vary significantly (±5 °C) from the values quoted.

Analysis of sample gas and treatment of the data at ANU were similar to that described by Dunlap *et al*. (1995). At UCLA, sample gas was analyzed on a VG3600 mass spectrometer. After active gases were removed by a Zr-Al getter (AP-10) operating at ~700°C on the extraction line, all five isotopes of Ar were measured. Ion-beam measurement was through both a Daly photomultiplier and a Faraday cup, depending on beam intensity, and the signal was measured using a digital electrometer with a 1x1011 ohm resistor. The sensitivity was about 2 x 10-15 mol/mV of ^{40}Ar on the Faraday, with a typical gain of 100 measured for each analysis on the Daly photomultiplier. The Daly/Axial gain for masses 38-36 was calculated from the gain measured on mass 39 and the mass discrimination on each detector. Correction factors for Ar produced in the reactor from K and Ca were determined from analysis of the salts enclosed with the irradiation package (Tables 3 and 4). J factors for sample aliquots were determined by curve fitting of the fluence monitor data. Decay constants and abundance of 40K recommended by the IUGS Subcommission on Geochronology were used (Steiger and Jäger, 1977).

Rb-Ar dating was carried out by Roland Maas at La Trobe University, Melbourne, Australia. After cleaning the white mica concentrates with distilled acetone and Milli-Q water in an ultrasonicator the fluid was removed and the mica flakes were rinsed repeatedly with fresh Milli-Q water. The samples were weighed (about 30 mg) then spiked with a mixed 87Rb-84Sr spike and dissolved in a Savillex beaker using HF-HNO3, followed by 6M HCl. The dried chlorides were redissolved in 3M HNO3 and loaded onto 0.1 ml beds of pre-cleaned EICHROM Sr spec resin. Rb and matrix elements were collected and stored. Sr was eluted in Milli-Q water, dried and passed over the column a second time. Sr was loaded onto single Ta filaments as a phosphate and analysed on a Finnigan-MAT 262 in static mode. Mass fractionation was corrected by normalizing to 88Sr/86Sr=8.37521. The SRM987 standard gave 0.71023 ± 4 (2>s). Rb was leached from the matrix residue with Milli-Q water, loaded onto a double Ta filament and run in single collector peak switching mode. Feldspar standard SRM607 gave a model age of 1417 ± 10 Ma (initial ratio = 0.710) using the same spike solution that was used for the white micas. This compares well with a model age calculated from the certified data (1410 Ma).

One point isochrones were calculated using an IR of 0.710; input 2 sigma errors were 0.5% for 87Rb/86Sr and 0.01% for 87Sr/86Sr.

Table 4: 40Ar/39Ar Step-Heating Data for Forlandsundet Basin Micas

$^{40}Ar/^{39}Ar$	$^{38}Ar/^{39}Ar$ (10^{-2})	$^{37}Ar/^{39}Ar$ (10^{-2})	$^{36}Ar/^{39}Ar$ (10^{-3})	^{39}Ar (10^{-14} mol)	Cumulative ^{39}Ar (%)	$\%^{40}Ar^*$	$^{40}Ar^*/^{39}Ar_K$	Calculated Age (Ma) ± 1 s.d.	K/Ca
108 White Mica, 10-38 μm, J = 0.006925 ± 0.57%									
41.87	5.14	24.62	116	1.61	1.87	18.5	7.728	94.2 ± 6.1	2.0
13.48	2.35	22.96	6.90	1.99	4.17	84.8	11.44	137.6 ± 0.8	2.2
19.59	2.22	40.68	5.53	4.02	8.83	91.7	17.96	211.7 ± 0.8	1.2
26.04	1.45	79.07	2.96	8.33	18.5	96.8	25.21	290.6 ± 0.5	0.6
31.02	1.24	6.68	2.07	5.82	25.2	98.0	30.39	344.9 ± 0.4	7.4
33.98	1.25	3.09	1.85	9.24	36.0	98.3	33.41	375.8 ± 0.3	16
36.41	1.30	3.02	2.41	6.60	43.6	98.0	35.68	398.7 ± 0.5	16
39.48	1.29	2.62	3.31	8.34	53.3	97.5	38.48	426.5 ± 0.4	19
41.23	1.27	2.04	3.57	8.46	63.1	97.4	40.15	443.0 ± 0.5	24
41.88	1.27	1.58	2.79	10.6	75.4	98.0	41.03	451.6 ± 0.7	31
43.31	1.29	1.78	2.45	12.3	89.6	98.3	42.56	466.4 ± 0.4	28
45.94	1.42	4.64	5.41	5.81	96.4	96.5	44.32	483.3 ± 0.6	11
57.46	3.22	47.47	46.8	3.13	100	76.0	43.66	477.0 ± 1.9	1.0
						Totals	35.38	395.3 ± 0.7	25

$^{40}Ar/^{39}Ar$	$^{37}Ar/^{39}Ar$ (10^{-2})	$^{36}Ar/^{39}Ar$ (10^{-3})	^{39}Ar (10^{-14} mol)	Cumulative ^{39}Ar (%)	$\%^{40}Ar^*$	$^{40}Ar^*/^{39}Ar_K$	Calculated Age (Ma) ± 1 s.d.	K/Ca

108 White Mica, <2 μm, J = 0.005704 ± 0.4%

22.81	0.7587	28.95	4.46	3.8	62.3	14.22	140.7 ± 2.7	69
20.53	0.2557	13.41	4.81	7.8	80.6	16.54	162.6 ± 1.6	206
22.67	0.2814	7.730	8.08	14.7	89.8	20.36	198.2 ± 1.8	187
24.33	0.2400	5.569	13.1	25.7	93.1	22.65	219.2 ± 1.3	219
29.12	0.0011	3.562	29.4	50.6	96.3	28.03	267.6 ± 0.6	-
33.44	0.6619	3.283	7.87	57.2	97.0	32.44	306.3 ± 1.1	79
34.72	0.5593	2.159	9.04	64.9	98.1	34.05	320.2 ± 2.4	94
36.88	0.3826	2.610	9.55	72.9	97.8	36.08	337.6 ± 1.6	138
38.61	0.9911	4.284	9.03	80.6	96.6	37.32	348.2 ± 1.2	53
39.61	1.061	2.834	7.22	86.7	97.8	38.74	360.2 ± 0.7	50
38.69	2.019	3.471	6.53	92.2	97.3	37.64	350.9 ± 2.2	26
37.89	4.421	3.089	3.10	94.8	97.5	36.95	345.0 ± 4.7	12
38.16	18.39	5.445	2.06	96.5	95.8	36.53	341.5 ± 3.7	2.9
36.43	24.01	11.18	1.48	97.8	90.9	33.12	312.2 ± 2.3	2.2
29.42	91.41	9.068	2.63	100.0	91.1	26.83	256.9 ± 3.5	0.6
					Totals	29.64	281.8 ± 1.5	80

108 White Mica, 2-6 μm, J = 0.005747 ± 0.4%

21.83	0.06159	3.110	3.28	3.4	57.8	12.60	126.1 ± 3.1	855
23.88	0.8157	1.812	2.55	6.0	77.5	18.49	182.2 ± 6.6	65
25.88	0.8739	1.655	5.95	12.1	81.0	20.94	205.0 ± 2.0	60
24.97	1.863	0.3725	7.57	19.8	95.5	23.87	231.9 ± 1.8	28
29.10	0.2748	0.3279	11.1	31.2	96.6	28.11	270.2 ± 0.5	192
33.06	0.1136	0.1800	8.50	39.9	98.3	32.50	309.0 ± 1.5	463
36.31	0.7777	0.1654	9.31	49.4	98.6	35.72	336.8 ± 1.3	68
39.33	0.0213	0.05973	9.61	59.2	99.5	39.13	366.0 ± 1.1	2463
41.87	0.5542	0.2759	8.12	67.5	98.0	40.99	381.7 ± 1.9	95
43.12	0.8173	0.0829	8.21	75.9	99.4	42.85	397.2 ± 0.9	65
42.88	0.8931	0.1387	7.86	84.0	99.0	42.44	393.8 ± 1.7	59
42.79	1.736	0.1954	9.16	93.4	98.6	42.14	391.3 ± 1.1	30
40.83	20.80	0.4068	6.49	100.0	97.0	39.64	370.3 ± 1.7	2.5
					Totals	34.31	324.7 ± 1.6	368

$^{40}Ar/^{39}Ar$	$^{38}Ar/^{39}Ar$ (10^{-2})	$^{37}Ar/^{39}Ar$ (10^{-2})	$^{36}Ar/^{39}Ar$ (10^{-3})	^{39}Ar (10^{-14} mol)	Cumulative ^{39}Ar (%)	$\%^{40}Ar^*$	$^{40}Ar^*/^{39}Ar_K$	Calculated Age (Ma) ± 1 s.d.	K/Ca

232 White Mica, 10-38 μm, J = 0.006923 ± 0.29%

192.0	22.54	3.842	627.3	0.300	0.37	3.47	6.665	81.4 ± 15.1	13
87.44	10.85	2.957	271.3	0.976	1.57	8.30	7.258	88.4 ± 5.1	17
68.08	7.536	2.820	206.9	1.47	3.38	10.2	6.929	84.5 ± 3.7	18
26.59	2.876	2.554	50.24	4.57	9.00	44.1	11.72	140.7 ± 1.6	19
18.86	1.510	2.375	4.370	8.50	19.5	93.0	17.54	206.8 ± 0.3	21
26.64	1.291	1.909	3.155	10.9	32.9	96.4	25.69	295.3 ± 0.2	26
34.75	1.243	1.561	2.972	10.6	46.0	97.4	33.85	379.8 ± 0.5	32
41.12	1.260	1.325	3.705	7.71	55.5	97.3	40.00	441.0 ± 0.7	37
46.21	1.292	1.184	5.960	6.55	63.5	96.1	44.42	483.7 ± 0.6	42
50.53	1.387	1.101	10.35	6.27	71.3	93.9	47.45	512.4 ± 0.7	45
54.22	1.423	0.9858	12.63	6.64	79.4	93.1	50.47	540.6 ± 1.1	50
52.99	1.352	0.8306	7.991	6.66	87.6	95.5	50.61	541.9 ± 0.7	60
51.82	1.249	0.7051	2.470	5.28	94.1	98.5	51.06	546.1 ± 0.9	70
50.74	1.273	0.8535	1.871	3.14	98.0	98.9	50.16	537.8 ± 2.4	58
53.13	2.339	3.246	25.91	1.62	100	85.5	45.46	493.6 ± 3.5	15
						Totals	36.09	402.4 ± 0.9	38

232 White Mica, 38-75 μm, J = 0.006922 ± 0.24%

82.48	7.271	1.014	267.6	0.741	0.77	4.09	3.376	41.7 ± 11.7	49
22.83	2.595	1.023	54.26	1.85	2.70	29.7	6.770	82.6 ± 2.1	48
9.449	1.486	1.082	1.637	4.45	7.34	94.6	8.941	108.3 ± 0.2	46
12.26	1.474	1.073	0.8848	8.01	15.7	97.7	11.98	143.7 ± 0.2	46
18.19	1.231	0.8170	0.6724	11.4	27.6	98.8	17.96	211.4 ± 0.2	61
23.63	1.209	0.6868	0.6177	11.8	39.9	99.1	23.42	271.0 ± 0.2	72
28.28	1.198	0.5823	0.5416	10.2	50.5	99.3	28.09	320.6 ± 0.3	85
32.51	1.187	0.4945	0.4753	8.52	59.4	99.5	32.34	364.5 ± 0.4	100
36.79	1.202	0.4320	0.5126	8.93	68.7	99.5	36.62	407.6 ± 0.6	115
42.62	1.209	0.3804	0.6444	6.78	75.8	99.5	42.40	464.3 ± 0.3	130
47.76	1.228	0.3744	0.7061	5.62	81.6	99.5	47.53	513.1 ± 0.7	132
51.46	1.230	0.4460	0.7838	5.08	87.0	99.5	51.20	547.3 ± 0.5	111
54.78	1.243	0.7306	0.9622	4.21	91.3	99.4	54.47	577.2 ± 0.7	68
58.11	1.474	7.468	4.882	8.30	100	97.5	56.65	596.9 ± 0.5	6.6
						Totals	31.66	357.5 ± 0.5	78

236 White Mica, 10-38 μm, J = 0.006936 ± 0.41%

21.83	2.365	0.3664	45.14	3.51	2.75	38.8	8.468	103.0 ± 1.7	135
11.88	1.590	0.3669	4.375	4.84	6.53	88.9	10.57	127.6 ± 0.3	135
14.23	1.486	0.3403	2.358	11.5	15.5	94.9	13.51	161.6 ± 0.2	145
18.02	1.244	0.2364	1.688	11.7	24.7	97.1	17.49	206.6 ± 0.2	209
22.09	1.207	0.1780	1.720	20.9	41.0	97.6	21.56	251.4 ± 0.4	278
25.39	1.214	0.1598	2.149	10.1	48.9	97.4	24.73	285.6 ± 0.3	310
29.23	1.254	0.1506	3.696	16.1	61.5	96.2	28.11	321.4 ± 0.4	329
35.51	1.318	0.1245	7.157	12.3	71.1	94.0	33.37	375.6 ± 0.5	397
42.24	1.428	0.1546	11.61	10.4	79.2	91.8	38.78	429.8 ± 0.5	320
44.00	1.299	0.1466	4.307	7.57	85.1	97.1	42.70	468.0 ± 0.5	338
46.47	1.258	0.2044	1.568	10.6	93.4	98.9	45.98	499.4 ± 0.5	242
47.84	1.297	0.3441	1.814	4.02	96.5	98.8	47.28	511.7 ± 1.4	144
56.40	2.436	1.384	39.86	4.42	100	79.1	44.59	486.2 ± 2.2	36
						Totals	28.17	322.0 ± 0.5	262

329 White Mica, 10-38 μm, J = 0.006937 ± 0.33%

25.02	3.870	6.123	62.71	2.64	2.26	25.9	6.474	79.3 ± 0.8	8.1
15.69	2.461	12.37	27.92	5.77	7.21	47.3	7.424	90.6 ± 0.9	4.0
12.20	1.617	4.677	3.398	8.25	14.3	91.6	11.17	134.7 ± 0.1	11
17.98	1.634	15.73	2.731	12.0	24.6	95.4	17.17	203.0 ± 0.2	3.1
26.95	1.418	25.37	2.358	10.8	33.8	97.4	26.25	301.8 ± 0.2	2.0
33.02	1.311	11.23	1.834	12.0	44.1	98.3	32.46	366.4 ± 0.4	4.4
36.88	1.242	1.507	1.546	9.15	51.9	98.7	36.40	406.2 ± 0.2	33
39.11	1.242	1.332	1.470	9.10	59.7	98.8	38.65	428.5 ± 0.3	37
40.81	1.275	1.224	1.724	9.10	67.5	98.7	40.27	444.5 ± 0.4	40
43.25	1.266	0.9687	1.835	9.75	75.9	98.7	42.69	467.9 ± 0.5	51
45.12	1.276	1.027	1.699	6.77	81.7	98.8	44.59	486.2 ± 0.5	48
46.32	1.300	1.295	1.354	5.60	86.5	99.1	45.89	498.6 ± 0.7	38
47.33	1.325	1.955	1.542	5.85	91.5	99.0	46.85	507.7 ± 0.7	25
47.46	2.541	14.74	14.41	9.92	100	91.0	43.19	472.8 ± 0.6	3.4
						Totals	32.21	363.8 ± 0.4	21

$^{40}Ar/^{39}Ar$	$^{38}Ar/^{39}Ar$ (10^{-2})	$^{37}Ar/^{39}Ar$ (10^{-2})	$^{36}Ar/^{39}Ar$ (10^{-3})	^{39}Ar (10^{-14} mol)	Cumulative ^{39}Ar (%)	$\%^{40}Ar^*$	$^{40}Ar^*/^{39}Ar_K$	Calculated Age (Ma) ± 1 s.d.	K/Ca

444A White Mica, 10-38 μm, J = 0.006926 ± 0.42%

52.41	7.819	1.617	152.3	2.50	1.56	14.1	7.374	89.9 ± 4.1	31
11.30	4.071	1.749	3.180	5.04	4.71	91.5	10.34	124.8 ± 0.3	28
17.08	3.410	1.989	2.322	6.78	8.95	95.8	16.37	193.7 ± 0.2	25
25.48	1.384	0.6667	0.9407	19.1	20.9	98.8	25.18	290.0 ± 0.3	74
31.93	1.315	0.4472	0.7544	23.7	35.7	99.2	31.68	357.9 ± 0.3	111
37.00	1.323	0.3635	0.8491	25.3	51.5	99.3	36.72	408.8 ± 0.4	136
39.58	1.284	0.3120	1.271	15.5	61.2	99.0	39.18	433.1 ± 0.5	159
40.65	1.300	0.2986	1.623	16.9	71.7	98.8	40.15	442.6 ± 0.4	166
41.68	1.303	0.3707	1.717	24.4	86.9	98.7	41.15	452.4 ± 0.4	134
42.57	1.367	0.5917	2.182	16.9	97.5	98.4	41.90	459.7 ± 0.5	84
65.31	3.996	11.09	76.09	4.04	100	65.5	42.81	468.5 ± 0.5	4.5
						Totals	34.42	385.7 ± 0.5	111

444A White Mica, 38-53 μm, J = 0.006927 ± 0.47%

51.43	7.174	1.712	153.3	2.02	1.54	11.9	6.106	74.7 ± 4.8	29
9.943	3.984	2.015	3.597	3.68	4.35	89.1	8.856	107.4 ± 0.3	25
14.15	4.021	2.327	2.376	4.76	7.98	94.9	13.42	160.4 ± 0.3	21
19.79	1.891	1.161	1.183	8.69	14.6	98.1	19.41	227.6 ± 0.2	43
25.37	1.317	0.6052	0.7884	14.6	25.7	99.0	25.11	289.3 ± 0.3	82
30.45	1.319	0.4733	0.7658	14.9	37.1	99.2	30.20	342.7 ± 0.3	105
34.85	1.336	0.3984	0.7030	13.7	47.5	99.3	34.62	387.8 ± 0.3	124
38.23	1.309	0.3370	0.9838	12.1	56.8	99.2	37.92	420.7 ± 0.3	147
40.06	1.307	0.3242	1.555	7.66	62.6	98.8	39.57	437.1 ± 0.6	153
40.78	1.320	0.3322	1.792	8.76	69.3	98.6	40.23	443.5 ± 0.5	149
41.61	1.326	0.3733	1.975	12.2	78.6	98.5	41.00	451.0 ± 0.4	133
42.15	1.373	0.4581	2.170	9.73	86.0	98.4	41.49	455.7 ± 0.5	108
42.98	1.438	0.6688	2.696	9.04	92.9	98.1	42.16	462.2 ± 1.4	74
54.08	3.368	10.72	39.35	9.29	100	78.5	42.44	464.9 ± 1.1	4.6
						Totals	33.27	374.1 ± 0.5	97

444A White Mica, 53-75 μm, J = 0.006924 ± 0.33%

13.35	4.391	1.858	19.59	3.85	3.50	56.5	7.541	91.8 ± 0.7	27
12.45	4.509	2.398	2.235	4.79	7.86	94.5	11.77	141.3 ± 0.3	21
18.48	2.100	1.237	1.115	8.88	15.9	98.1	18.13	213.3 ± 0.3	40
23.48	1.344	0.6008	0.6548	10.1	25.1	99.1	23.27	269.5 ± 0.2	82
27.34	1.314	0.4840	0.5947	9.60	33.9	99.3	27.14	310.7 ± 0.2	102
30.87	1.332	0.4319	0.5039	10.4	43.3	99.4	30.69	347.6 ± 0.2	115
34.43	1.355	0.3926	0.4780	11.3	53.6	99.5	34.26	384.0 ± 0.4	126
37.81	1.317	0.3503	0.4857	12.0	64.5	99.6	37.64	417.9 ± 0.4	141
39.46	1.312	0.3440	0.6915	9.79	73.4	99.4	39.23	433.5 ± 0.5	144
40.44	1.313	0.3572	0.7727	13.1	85.3	99.4	40.18	442.9 ± 0.5	139
41.20	1.342	0.4364	0.8461	9.49	94.0	99.3	40.93	450.1 ± 0.4	113
44.96	3.416	13.27	7.043	6.62	100	95.3	42.87	468.9 ± 1.7	3.7
						Totals	31.68	357.8 ± 0.4	100

444A White Mica, 75-150 μm, J = 0.006929 ± 0.51%

13.42	5.739	2.358	22.25	2.697	3.20	50.8	6.822	83.3 ± 0.4	21
11.85	7.936	4.100	3.595	2.589	6.28	90.8	10.77	129.8 ± 0.3	12
16.55	5.687	3.271	2.477	4.314	11.4	95.4	15.80	187.4 ± 0.3	15
21.22	2.163	1.141	0.9406	6.313	18.9	98.6	20.92	244.2 ± 0.5	43
25.82	1.448	0.5971	0.2779	7.292	27.6	99.6	25.72	295.8 ± 0.7	83
30.23	1.451	0.4987	0.4286	7.750	36.8	99.5	30.08	341.5 ± 0.4	99
34.13	1.482	0.4595	1.591	5.897	43.8	98.6	33.63	377.9 ± 0.5	108
36.30	1.495	0.5000	0.8081	4.258	48.8	99.3	36.04	402.2 ± 0.6	99
37.85	1.446	0.3952	1.207	4.057	53.6	99.0	37.47	416.4 ± 0.6	125
38.63	1.414	0.4221	0.9918	4.442	58.9	99.2	38.31	424.7 ± 1.0	117
39.31	1.405	0.5135	1.551	3.455	63.0	98.8	38.83	429.8 ± 0.6	96
39.71	1.352	0.3203	1.236	5.935	70.1	99.0	39.32	434.7 ± 0.8	155
41.13	1.386	0.4674	1.416	10.03	82.0	98.9	40.68	448.0 ± 1.1	106
42.40	1.549	0.8258	4.082	6.006	89.1	97.1	41.17	452.8 ± 0.5	60
63.98	5.302	14.06	72.85	9.183	100	66.3	42.45	465.1 ± 1.8	3.5
						Totals	32.70	368.4 ± 0.8	78

$^{40}Ar/^{39}Ar$	$^{38}Ar/^{39}Ar$ (10^{-2})	$^{37}Ar/^{39}Ar$ (10^{-2})	$^{36}Ar/^{39}Ar$ (10^{-3})	^{39}Ar (10^{-14} mol)	Cumulative ^{39}Ar (%)	$\%^{40}Ar^*$	$^{40}Ar^*/^{39}Ar_K$	Calculated Age (Ma) ± 1 s.d.	K/Ca

576 White Mica, 10-38 μm, J = 0.006933 ± 0.59%

109.3	17.76	5.008	349.7	0.296	0.22	5.5	5.986	73.4 ± 5.9	10
69.10	11.51	5.464	212.5	0.427	0.53	9.1	6.301	77.1 ± 3.9	9.1
56.93	8.170	5.502	166.7	1.04	1.30	13.4	7.648	93.2 ± 2.3	9.0
24.23	4.276	8.734	57.35	1.03	2.06	30.0	7.262	88.6 ± 4.5	5.7
10.86	2.295	15.30	6.547	2.75	4.10	82.1	8.908	108.1 ± 0.4	3.2
11.22	2.444	55.17	3.321	6.57	8.96	91.4	10.26	124.0 ± 0.2	0.9
13.61	1.490	59.07	1.828	10.5	16.7	96.2	13.09	156.7 ± 0.2	0.8
15.35	1.280	28.87	1.164	14.4	27.4	97.7	15.00	178.5 ± 0.1	1.7
17.18	1.212	1.470	0.8743	14.1	37.8	98.4	16.90	199.9 ± 0.1	34
19.21	1.219	1.003	0.8274	14.9	48.8	98.6	18.95	222.6 ± 0.2	49
21.80	1.223	0.9255	0.9177	16.8	61.2	98.6	21.50	250.7 ± 0.2	53
25.13	1.232	0.7050	1.0532	14.2	71.7	98.7	24.80	286.2 ± 0.3	70
27.27	1.249	0.5812	0.9943	13.8	81.9	98.8	26.96	309.1 ± 0.2	85
28.61	1.256	0.5004	0.8706	12.2	91.0	99.0	28.33	323.5 ± 0.6	99
30.46	1.262	0.5202	0.8828	12.0	99.8	99.1	30.17	342.7 ± 0.4	95
137.0	12.00	2.678	343.9	0.231	100	25.8	35.38	395.8 ± 60.3	18
						Totals	20.61	241.0 ± 0.4	49

577 White Mica, 10-38 μm, J = 0.006925 ± 0.57%

13.64	4.248	1.462	15.81	7.05	5.27	65.6	8.941	108.5 ± 0.6	34
16.68	2.501	1.467	1.654	5.57	9.43	96.9	16.17	191.6 ± 0.5	34
22.14	1.416	0.8092	0.9900	9.01	16.2	98.6	21.82	254.0 ± 0.3	61
26.41	1.300	0.5045	0.7450	13.1	26.0	99.1	26.16	300.6 ± 0.4	98
30.17	1.281	0.4018	0.6274	13.1	35.8	99.3	29.96	340.4 ± 0.4	123
33.25	1.295	0.3671	0.6229	12.6	45.2	99.4	33.05	372.0 ± 0.3	135
36.13	1.303	0.3285	0.5589	14.8	56.2	99.5	35.94	401.3 ± 0.3	151
38.66	1.275	0.2939	0.5976	15.0	67.4	99.5	38.45	426.2 ± 0.4	168
40.05	1.313	0.2907	0.7537	11.6	76.1	99.4	39.80	439.4 ± 0.5	170
40.95	1.293	0.2952	0.8947	13.7	86.3	99.3	40.66	447.9 ± 0.3	168
41.53	1.289	0.3177	0.8604	14.1	96.8	99.3	41.25	453.6 ± 0.3	156
45.02	3.328	4.579	6.812	4.28	100	95.5	42.99	470.4 ± 1.3	11
						Totals	32.81	369.4 ± 0.4	126

586 White Mica, 10-38 μm, J = 0.006935 ± 0.50%

65.41	5.715	2.355	193.8	2.07	2.14	12.4	8.136	99.0 ± 6.5	21
14.13	1.810	2.255	10.51	2.50	4.71	77.9	11.00	132.6 ± 0.8	22
15.61	1.473	1.668	4.624	6.25	11.1	91.1	14.21	169.6 ± 0.3	30
19.89	1.243	0.9862	2.803	9.13	20.6	95.7	19.04	223.7 ± 0.3	50
23.09	1.215	0.7010	2.277	10.4	31.3	97.0	22.39	260.4 ± 0.3	71
25.65	1.221	0.6905	2.561	8.95	40.5	97.0	24.87	287.1 ± 0.2	72
27.93	1.246	0.7509	3.286	9.96	50.8	96.4	26.94	309.0 ± 0.4	66
31.72	1.328	0.7577	5.760	11.4	62.5	94.6	29.99	340.9 ± 0.3	65
37.09	1.376	0.6518	10.49	7.47	70.2	91.6	33.96	381.6 ± 0.7	76
38.73	1.409	0.7465	11.16	8.98	79.5	91.4	35.41	396.1 ± 0.7	66
38.99	1.279	0.7715	4.286	7.42	87.1	96.7	37.70	419.0 ± 0.5	64
40.54	1.289	1.264	2.760	6.08	93.4	97.9	39.70	438.7 ± 0.7	39
49.92	1.916	5.084	20.69	6.44	100	87.7	43.79	478.4 ± 0.7	10
						Totals	28.31	323.4 ± 0.6	56